

Exponent[®]

Failure Analysis Associates

**PG&E Hydrotest Rupture
Line 300B Metallurgical
Examination**

**PG&E Hydrotest Rupture
Line 300B Metallurgical
Examination**

Prepared by

Exponent Failure Analysis Associates
149 Commonwealth Drive
Menlo Park, CA 94025

March 2012

Exponent, Inc.

Contents

	<u>Page</u>
Executive Summary	iii
Background	1
Visual and Non-Destructive Examination	2
Fractography	5
Metallographic Examination	17
Mechanical Testing	29
Chemical Analysis	35
Discussion and Conclusions	36
Limitations	38
 Appendix A Anamet Inc. Reports	

Executive Summary

Exponent Failure Analysis Associates (Exponent) was retained to help determine the cause of the October 24, 2011 Line-300B hydrotest rupture. Our metallurgical investigation was conducted by a group of Pacific Gas and Electric (PG&E), Kiefner and Associates, California Public Utilities Commission (CPUC) Consumer Products and Safety Division (CPSD), and Exponent personnel. The CPUC/CPSD was involved in all phases and the direction of our analysis. Our analysis included visual, dimensional, stereomicroscopic, scanning electron microscopic (SEM), and energy dispersive spectroscopic (EDS) analyses of the ruptured pipe section. Further, chemical analysis and mechanical testing of selected portions of the subject pipe were conducted for comparison with American Petroleum Institute (API) specifications.

Our analysis indicated that Line 300B ruptured during hydrotesting due to the existence of solidification cracking and lack-of-penetration weld discontinuities that were formed during original fabrication of the subject pipe section. Solidification cracking (also known as “hot-cracking”) occurred during welding of the outer submerged-arc weld pass. Solidification cracking occurs when the final solidifying metal cannot support the thermally or mechanically-induced strain from the welding process, and can be caused by poor joint restraint, improper welding parameters, and by interdendritic segregation of steel impurities (such as sulfur). Due to the proximity to a factory girth weld and associated “squirt” welds, the solidification cracking in the L-300B hydrotest failure may have been associated with cracking from poor restraint common at joint ends in early 1950-era double submerged arc-welds. Lack-of-penetration observed along the ruptured weld seam also contributed to the hydrotest rupture. The lack-of-penetration was caused by inner and outer weld misalignment, as well as small weld beads.

No evidence of any progressive fracture, such as fatigue or stress-corrosion cracking, was observed. Thus, the weld discontinuities responsible for the hydrotest rupture existed at the time Line 300B was originally installed, and did not propagate or grow during service. Mechanical testing indicated that base metal and weld samples meet current API specifications for X52 piping strength and ductility. Chemical analysis indicated the subject piping contained

carbon and sulfur levels that were acceptable when it was installed (for Grade X42, the only “high-test” grade available at the time), but exceed current API specifications for X52 piping.

Background

On October 24, 2011, Line 300B ruptured during PG&E Hydrotest T-117, conducted between Mile Positions 283.85 and 284.62. The rupture occurred at Mile Position 284.14 when the test pressure reached 998 psig (94.9-percent of specified-minimum yield stress (SMYS)), on the way to a maximum test-point pressure of 1048 psig. The break occurred 28 minutes into the hydrotest.

The portion of 300B tested in Hydrotest T-117 was 34-inch diameter, 0.344-inch nominal thickness, double-submerged arc welded (DSAW) pipe, made up of API X60, X52, and X48 sections. The ruptured portion of Line 300B was API X52 pipe, installed in 1950. The maximum allowable operating pressure (MAOP) of the subject line was 757 psig, or 71.94-percent of SMYS. Thus, the rupture occurred at a pressure approximately equal to 132-percent of MAOP.

Our analysis was conducted to determine the cause of the T-117 hydrotest rupture, and included visual and dimensional inspection at PG&E's San Ramon facility, fractographic and metallographic examination at Exponent's Menlo Park laboratory, as well as chemical analysis and mechanical testing at Anamet's laboratory in Hayward.

Visual and Non-Destructive Examination

The ruptured section of Line 300B ran in a primarily south-east to north-west orientation. For purposes of the investigation, the pipe upstream direction was designated as “East” and the downstream direction as “West.” The sides of the rupture were correspondingly designated as “North” and “South.” The rupture occurred approximately at the 12:00 clock position, primarily along the longitudinal DSAW seam, and was approximately seven inches in length overall, as shown in Figure 1. The origin was observed at the maximum rupture opening displacement location, shown in Figure 1, centered approximately 17 inches downstream from a factory-welded submerged-arc girth weld. Chevron marks were observed on either side of the origin, indicating its presence. The rupture extended both upstream and downstream from the origin. The east side of the rupture crossed the upstream girth weld and traveled through the base metal of the adjacent pipe section for approximately 19 inches before arresting. “Squirt” welds extended along the longitudinal seams approximately eight inches from either side of the upstream factory girth weld.

Visual inspection of the fracture surface indicated a darkened area along the outer diameter (OD) weld, located at the rupture area corresponding to the maximum opening, shown in Figure 2 and Figure 3. The darkened area was present on both North and South fracture faces, and extended for approximately seven inches. A relatively shiny strip of un-welded material was observed to extend roughly along the centerline of most of the rupture (not including the squirt weld area), shown in Figure 3. The strip was darkened throughout the origin area. This strip was consistent with lack-of-penetration between the inner and outer submerged arc welds.

Sections of the asphalt coating were removed and checked for asbestos content. Once the coating was confirmed not to contain significant asbestos, it was manually removed from the pipe section. The subject pipe was then grit blasted. Inside and outside pipe surfaces were visually inspected for any anomalies, such as seam or girth weld issues, cracks, wrinkles, corrosion damage, etc. Wet fluorescent magnetic-particle (WFMP) testing was conducted on the pipe exterior to find any surface-connected cracks. A few minor indications were observed and noted for further analysis.

“North” and “South” sections that included the rupture origin were removed from the subject pipe for fractographic examination. Several other sections from the subject pipe away from the rupture were removed for metallographic analysis, including a section of the girth weld near the rupture origin, a section of intact seam weld from west of the rupture, seam weld anomalies not associated with the failure, as well as anomalies observed from WFMP testing.

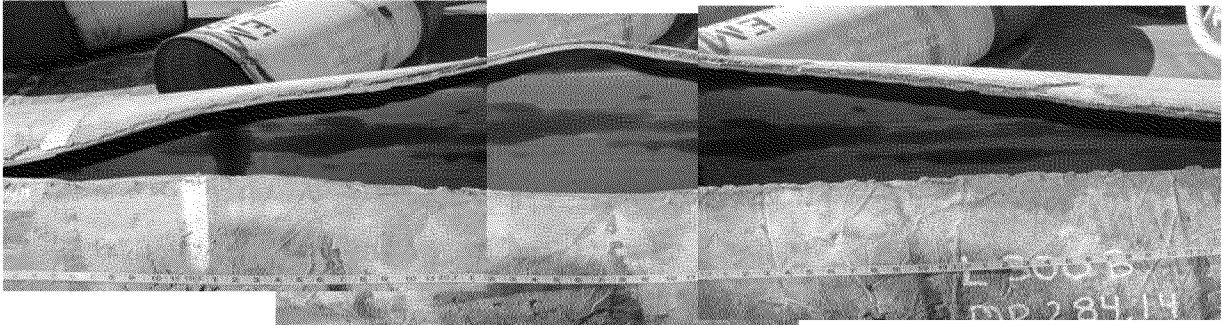


Figure 1. Montage of overall rupture.

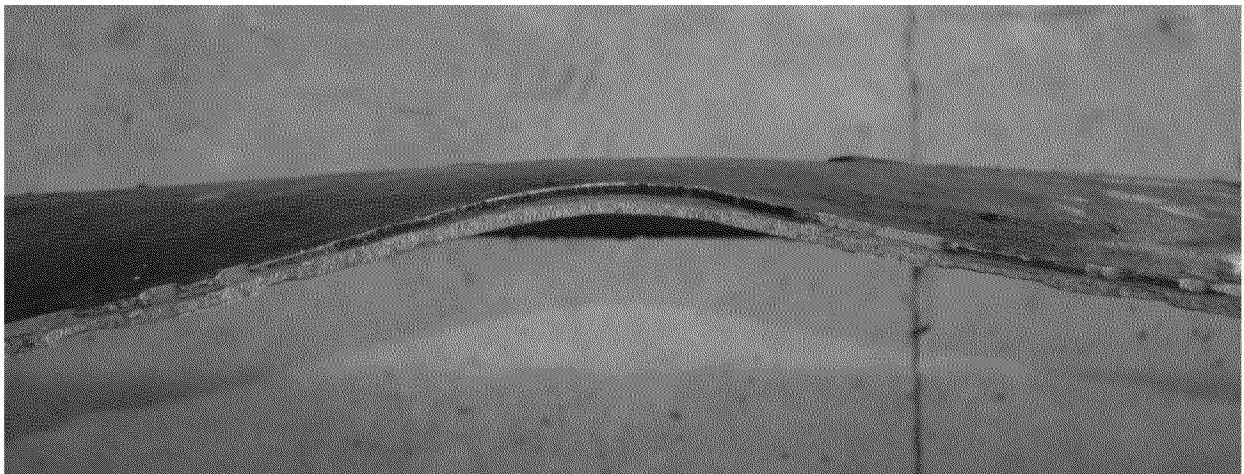


Figure 2. Photograph of the darkened area along the outer diameter (OD) weld at the rupture origin.

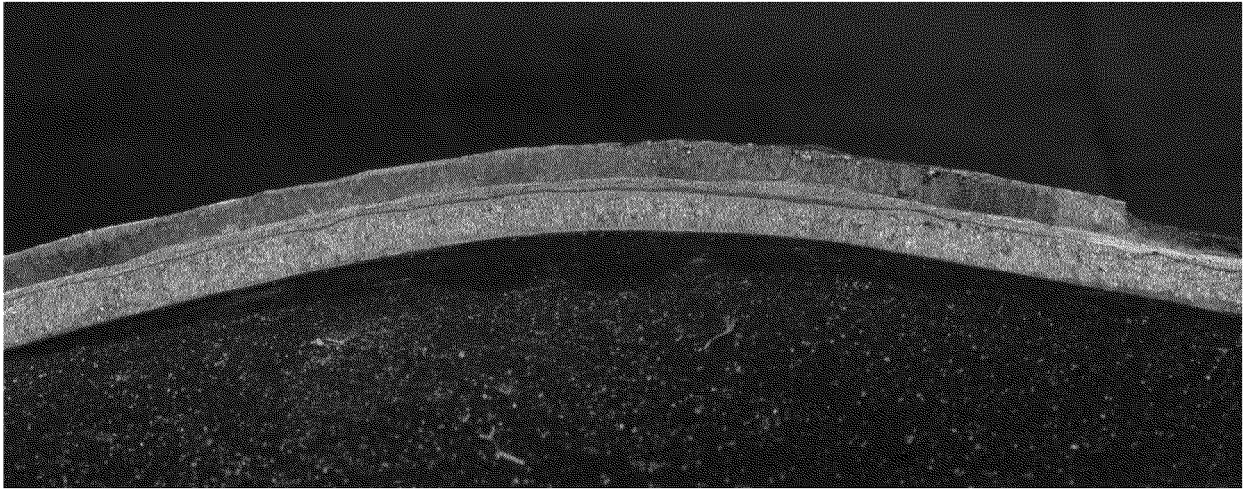


Figure 3. Photograph that shows the darkened OD weld region and the strip roughly along the centerline of the rupture.

Fractography

Fractographic analysis was conducted to help determine the cause of the rupture.

Approximately two feet of the rupture, including the origin, was removed from both sides of the break, shown in Figure 4. The middle of the two-foot sections contained the darkened fracture area. This area was removed from the north side of the break for cleaning, using acetone and ultrasound followed by SEM analysis, shown in Figure 5. A photographic montage of the darkened origin area after cleaning is shown in Figure 6.

The rupture origin, including the darkened area along the outside weld, was examined using SEM to allow identification of the fracture morphology. SEM analysis indicated that the darkened area exhibited interdendritic fracture morphology, consistent with cracking of the outside weld during final solidification (solidification cracking), also known as hot cracking, shown in Figure 7. The existence of solidification cracking indicates that this discontinuity had been present in the weld since the original manufacture of the pipe. The characteristic interdendritic cracking was observed over the entire darkened portion of the fracture surface. EDS of the interdendritic fracture area indicated elevated oxygen content compared to adjacent non-darkened areas, Figure 8. Thus, EDS results show that the dark coloration is consistent with the existence of an oxide layer. Dark-colored oxides on welded steel surfaces, such as observed at the fracture origin, are typically formed at the relatively high temperatures associated with welding. It is likely that the dark-colored oxide at the fracture origin formed during (or shortly after) the welding process, indicating that the solidification-crack discontinuity was exposed to oxygen during or shortly after welding.

SEM-based fractographic analysis was conducted to identify the fracture morphology for the remainder of the rupture origin. The inner diameter (ID) weld fracture primarily exhibited cleavage fracture morphology, shown in Figure 9, consistent with brittle fracture in steel. This cleavage fracture could have only occurred as a result of the hydrostatic rupture event. Microvoid coalescence morphology was observed at fracture surface locations along the inner and outer surfaces of the pipe, as well as along the weld discontinuity transitions within the pipe, shown in Figure 10. Microvoid coalescence morphology is indicative of ductile fracture in

steel. The lack-of-penetration area at the center of the pipe exhibited a relatively flat, featureless morphology, as expected, shown in Figure 11.

The rupture origin area was examined for any signs of progressive crack growth, such as by fatigue or stress corrosion cracking (SCC). The locations where progressive growth could have occurred were adjacent to the areas associated with solidification cracking or lack-of-penetration. Areas above and below these weld discontinuity zones were examined using SEM. The only fracture morphology observed above and below the solidification-cracking zone was microvoid coalescence, and only microvoid coalescence and cleavage fracture were observed to be adjacent to the lack-of-penetration zone, as shown in Figure 10 through Figure 13. As stated above, cleavage and microvoid coalescence fracture morphologies are associated with brittle and ductile fracture respectively, consistent with rupture during the hydrotest event. No evidence of morphology consistent with progressive crack growth, such as by fatigue or SCC was observed.

SEM analysis was also conducted to determine whether there was any communication between the observed solidification-cracking region and the pipe outer surface. If there was obvious communication, the solidification-cracking discontinuity may have been visible during external inspection. Our analysis showed that a small portion of the solidification-cracking region, approximately one-millimeter in length, may have contacted the outside surface of the weld, shown in Figure 14. The rest of the fracture area above the solidification cracking discontinuity exhibited microvoid coalescence fracture morphology. Due to the oxidation observed at the discontinuity, some portion of the solidification cracking must have been exposed to the outside environment while the metal was solidified.

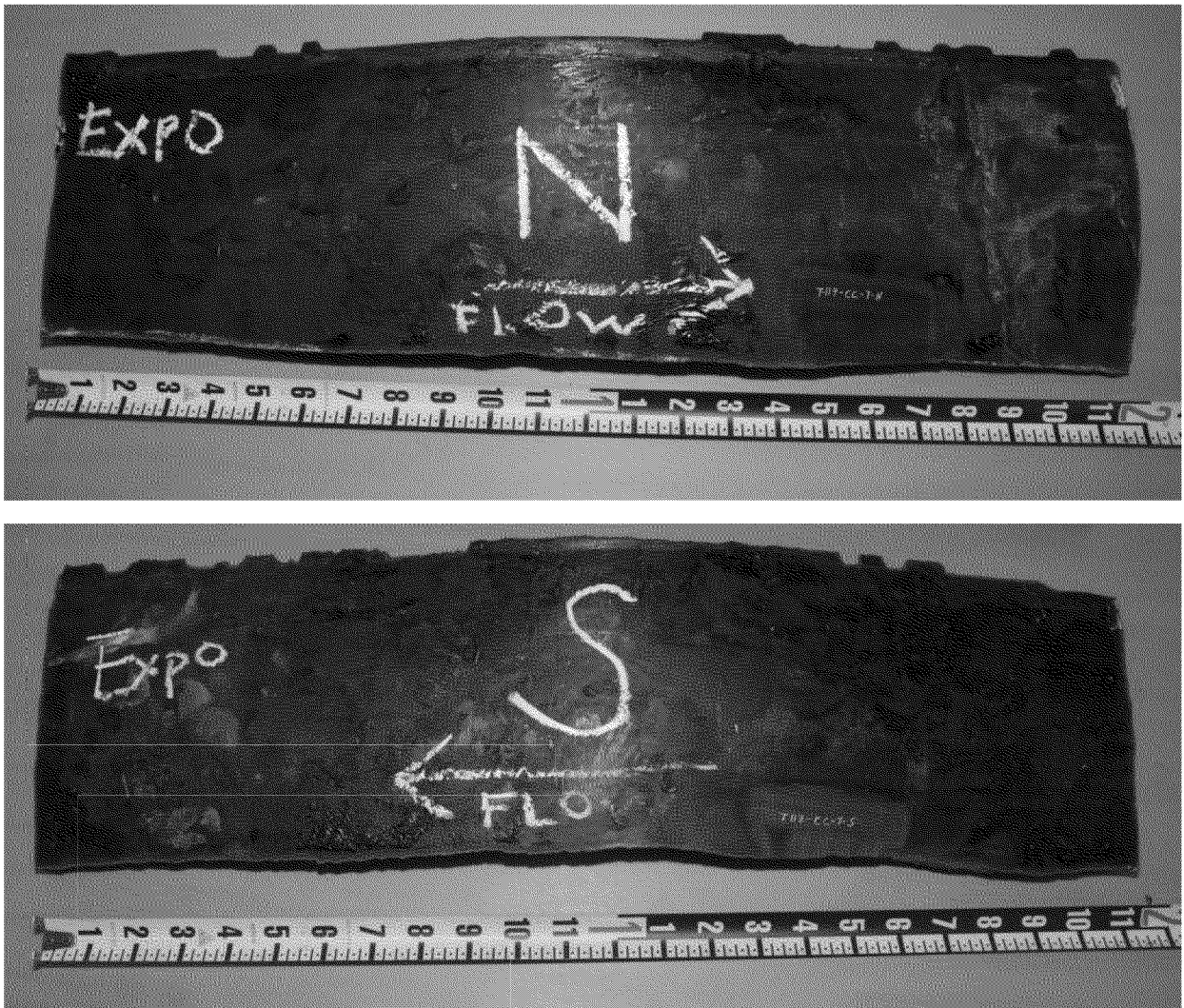


Figure 4. Images that show the two sections containing the rupture origin removed for analysis.



Figure 5. Image that shows the rupture origin section removed the north side, held adjacent to the south side.

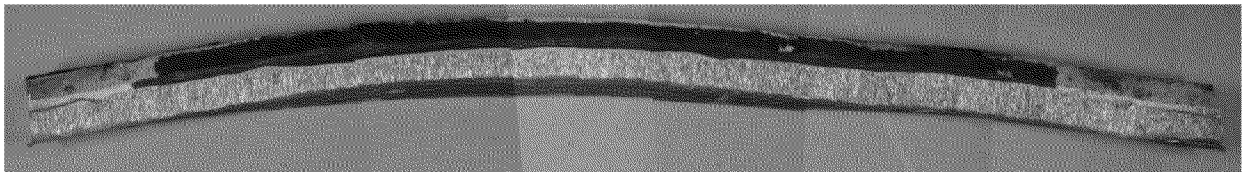


Figure 6. Photographic montage that shows the darkened region at the rupture origin after cleaning.

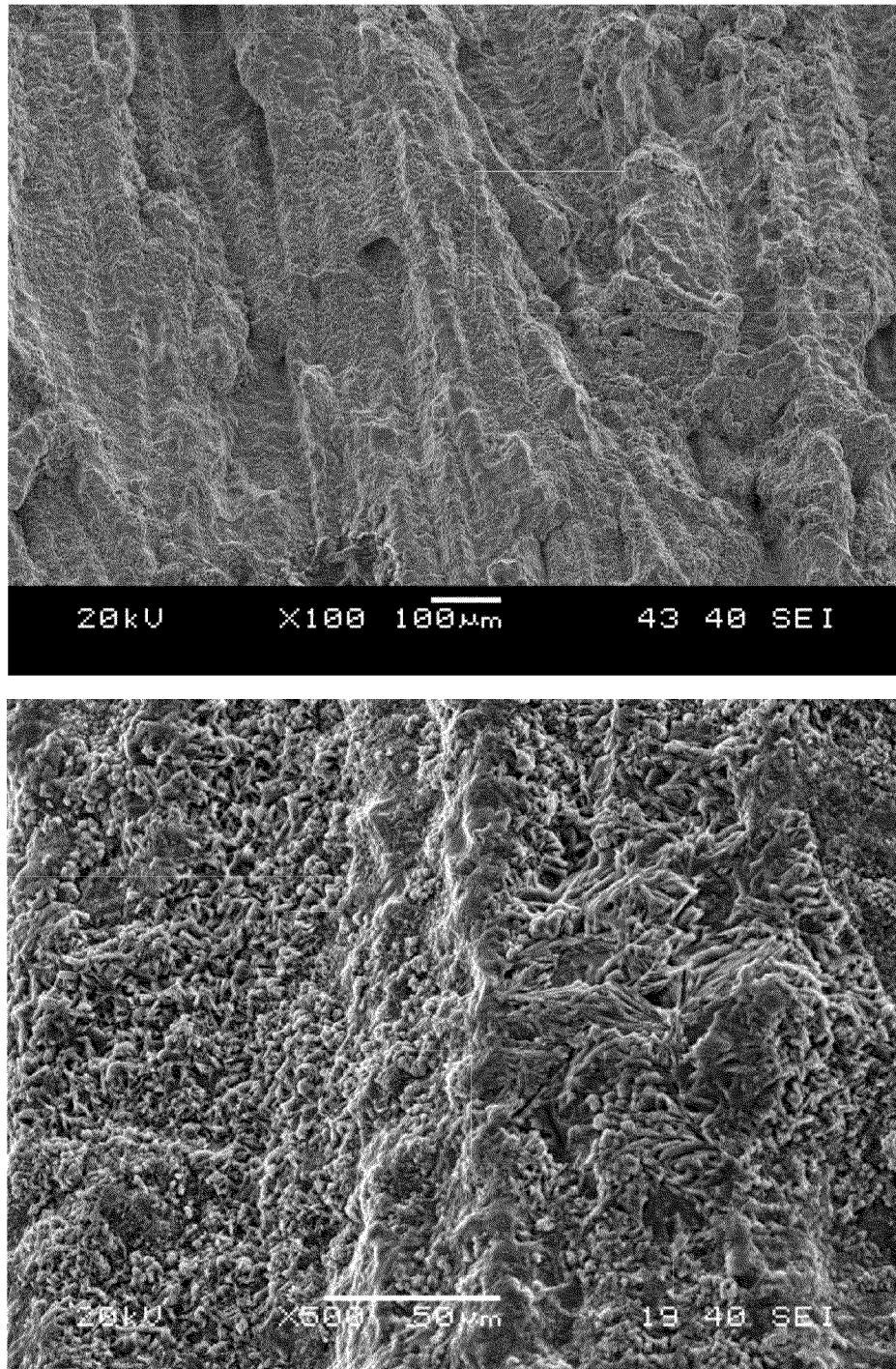


Figure 7. SEM images of the darkened area showing interdendritic fracture morphology, consistent with cracking of the outside weld during final solidification.

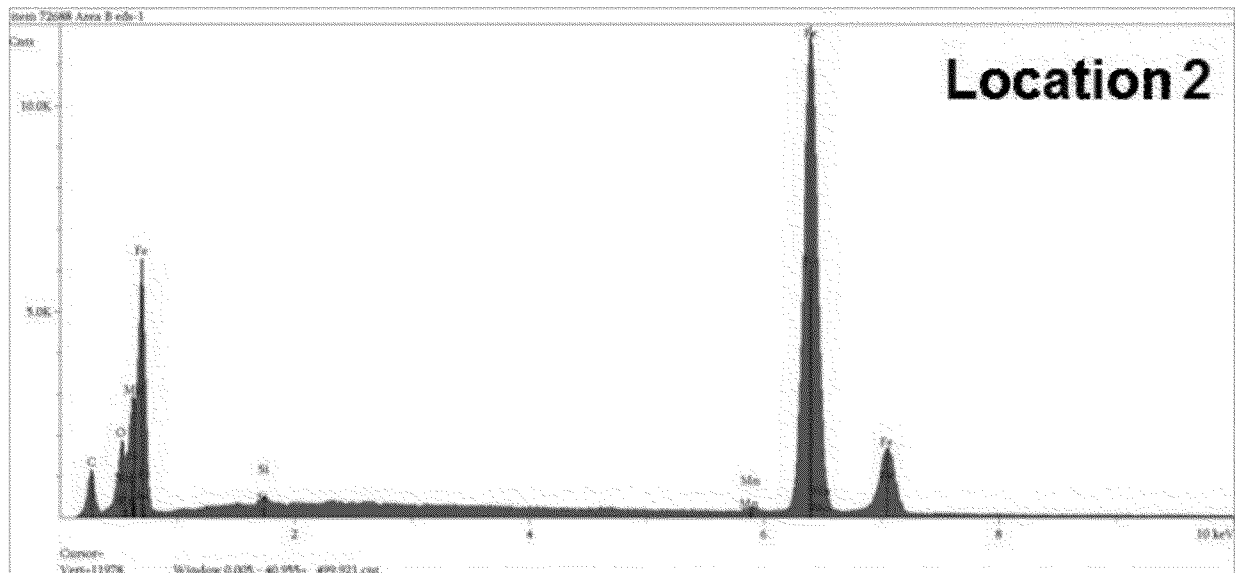
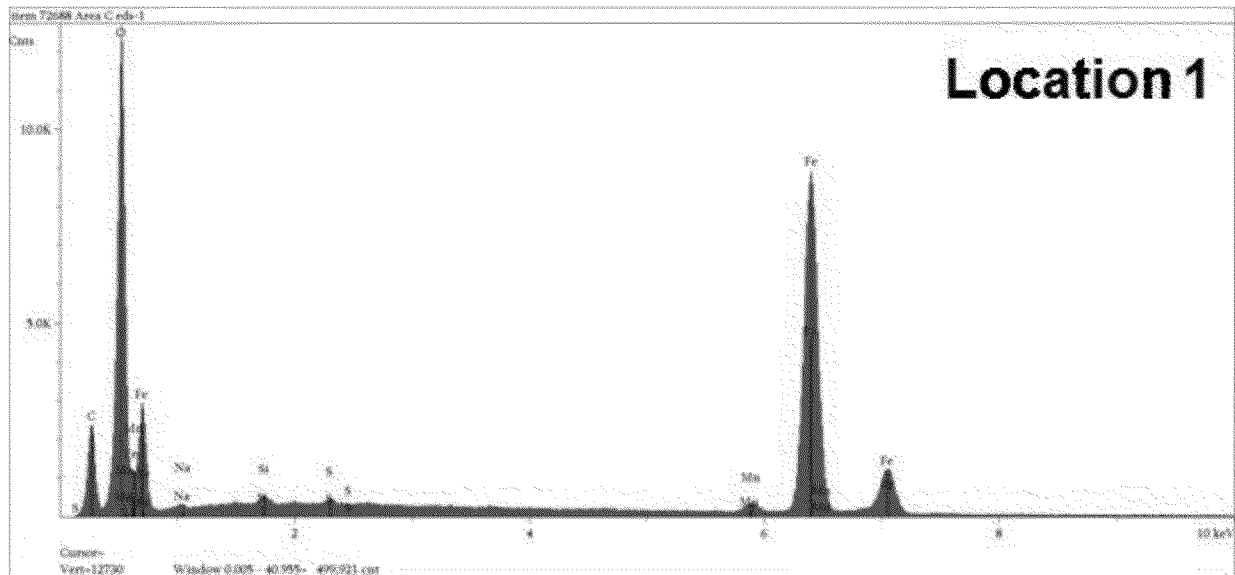
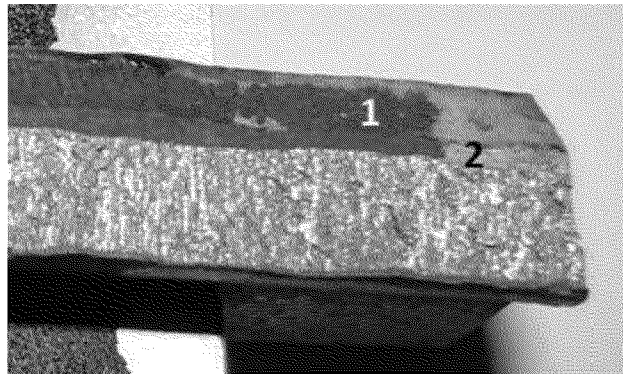


Figure 8. EDS spectra from the interdendritic fracture region (Location 1 in top image), that shows elevated oxygen content compared to an adjacent non-darkened fracture region (Location 2 in top image).

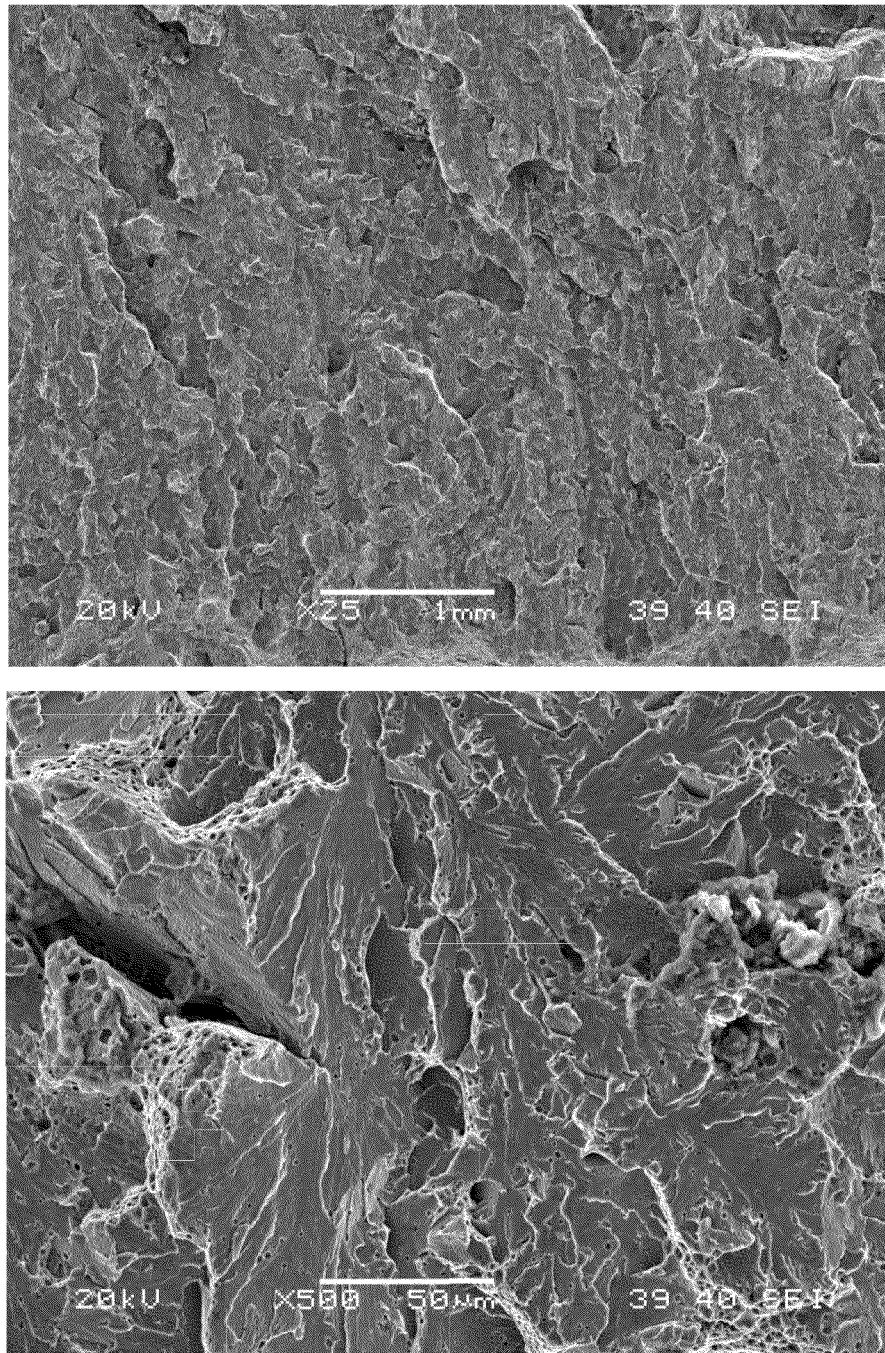


Figure 9. SEM images of the ID weld fracture surface that show cleavage fracture morphology.

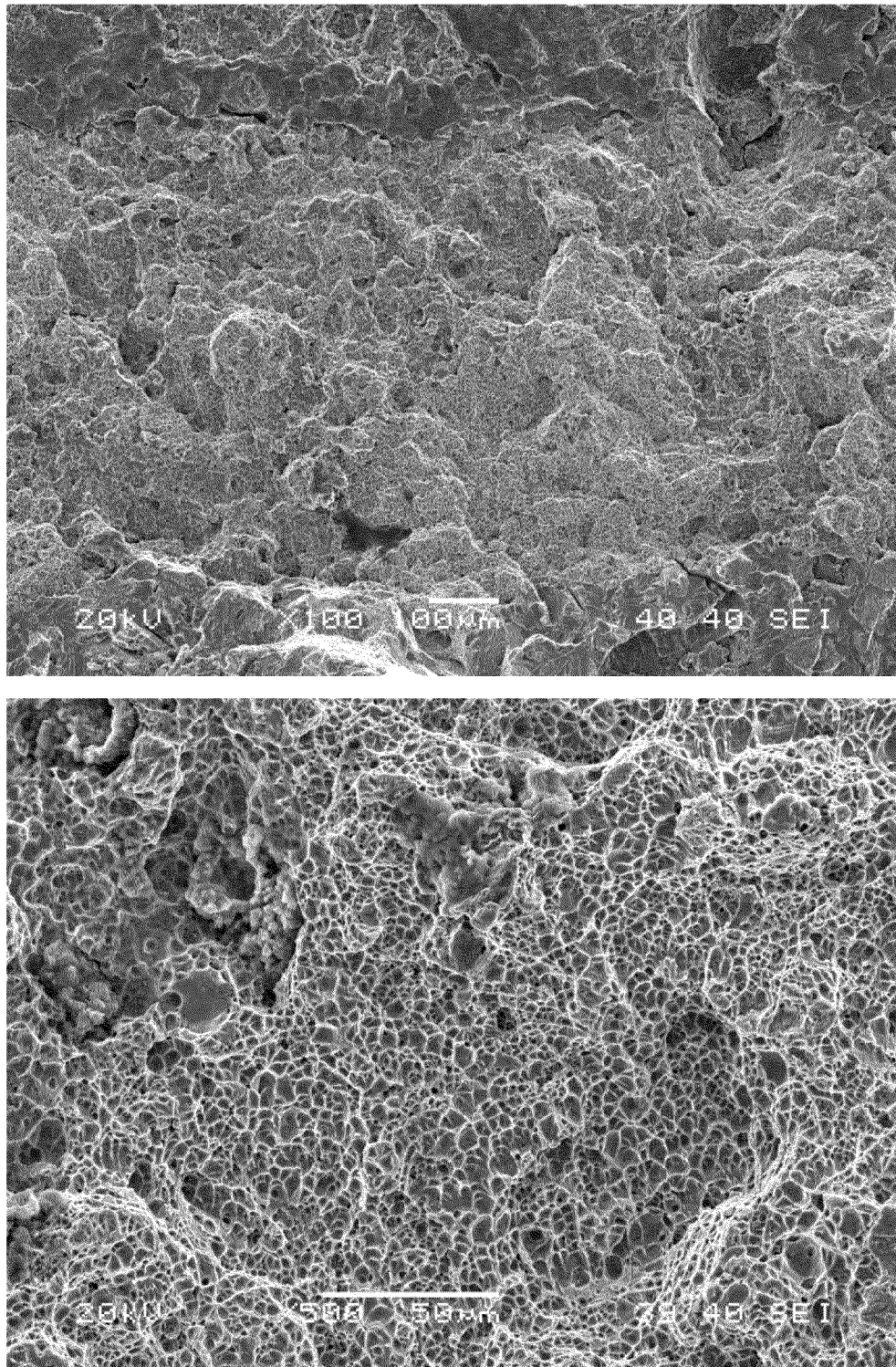


Figure 10. SEM images that show microvoid coalescence near the transition between the lack-of-penetration at the center of the pipe wall and the ID weld.

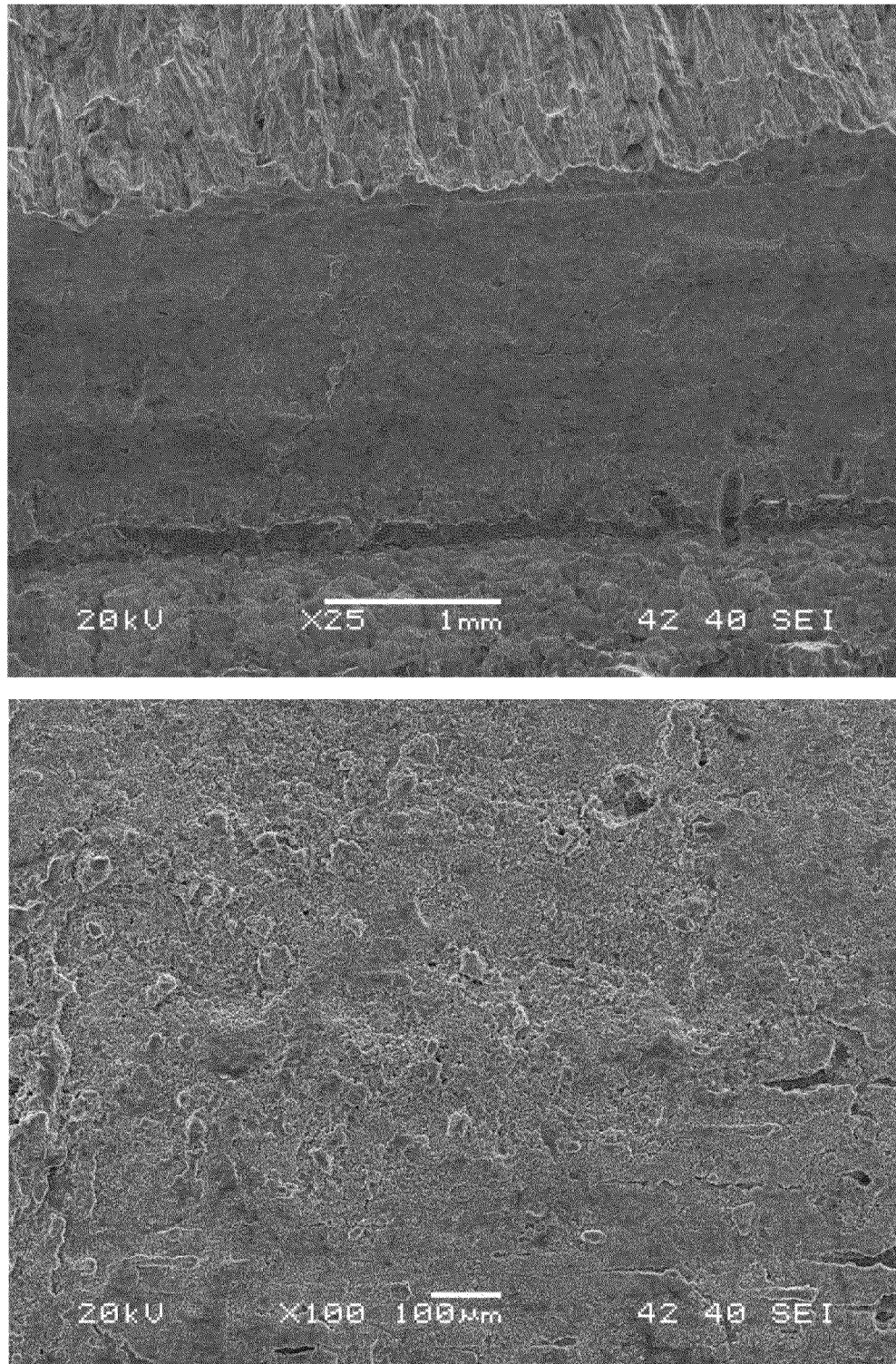


Figure 11. SEM images that show a relatively flat, featureless morphology at the lack-of-penetration area in the center of the pipe.

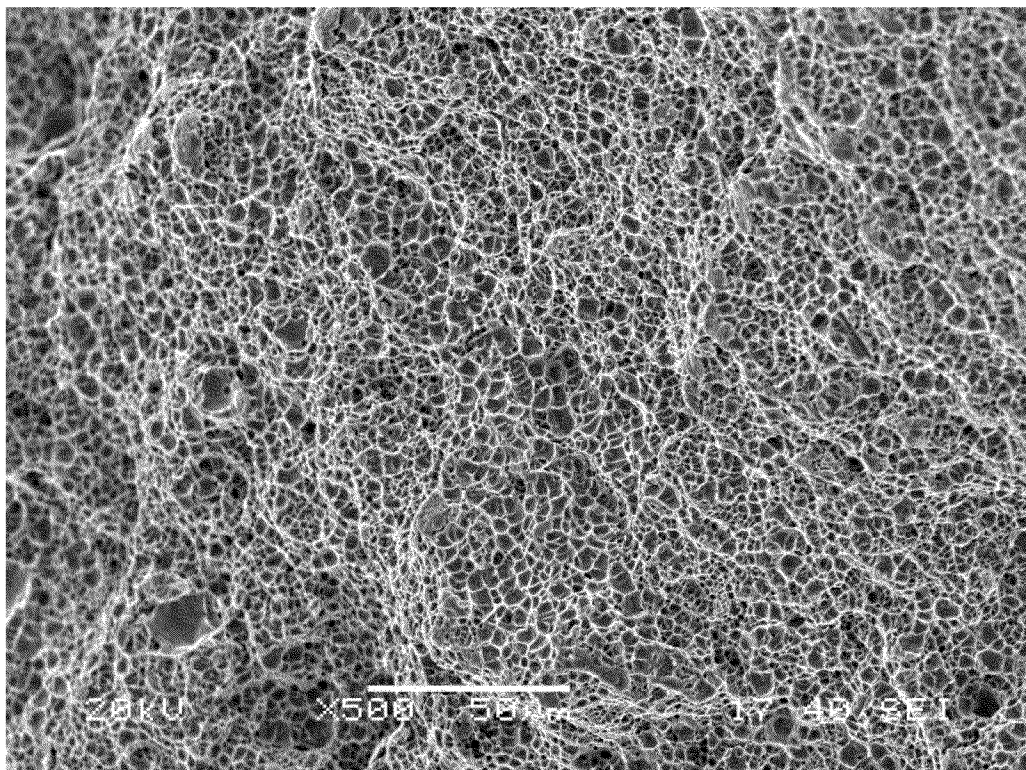
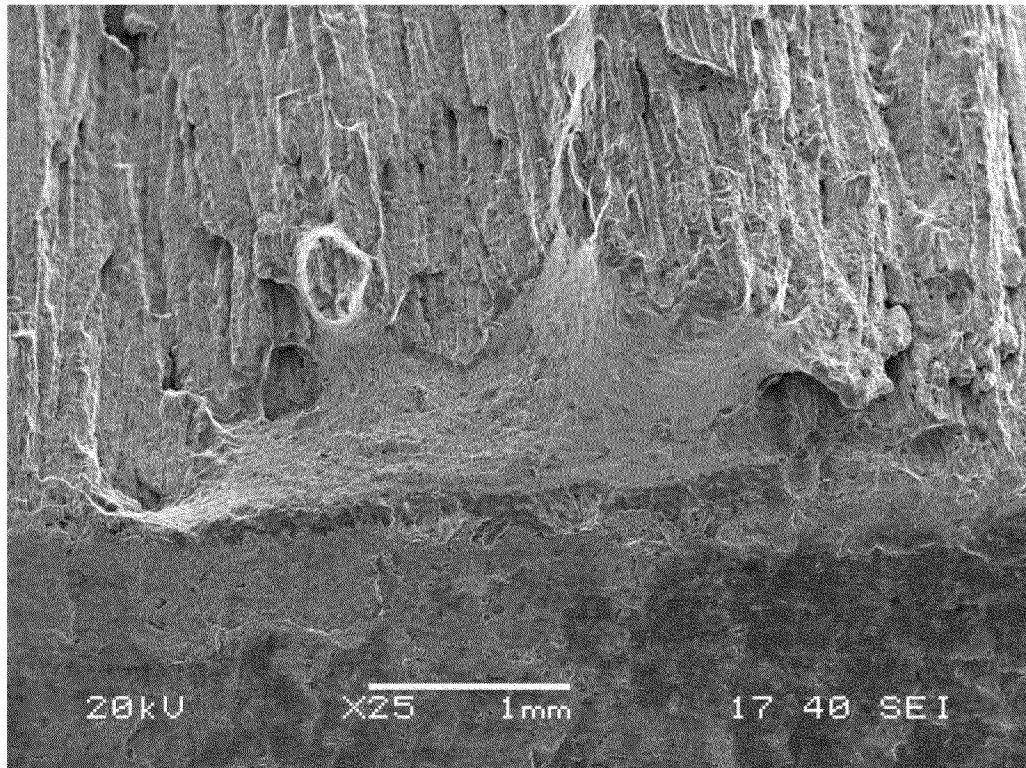


Figure 12. SEM images that show microvoid coalescence in the region between the solidification cracking and lack-of-penetration zones.

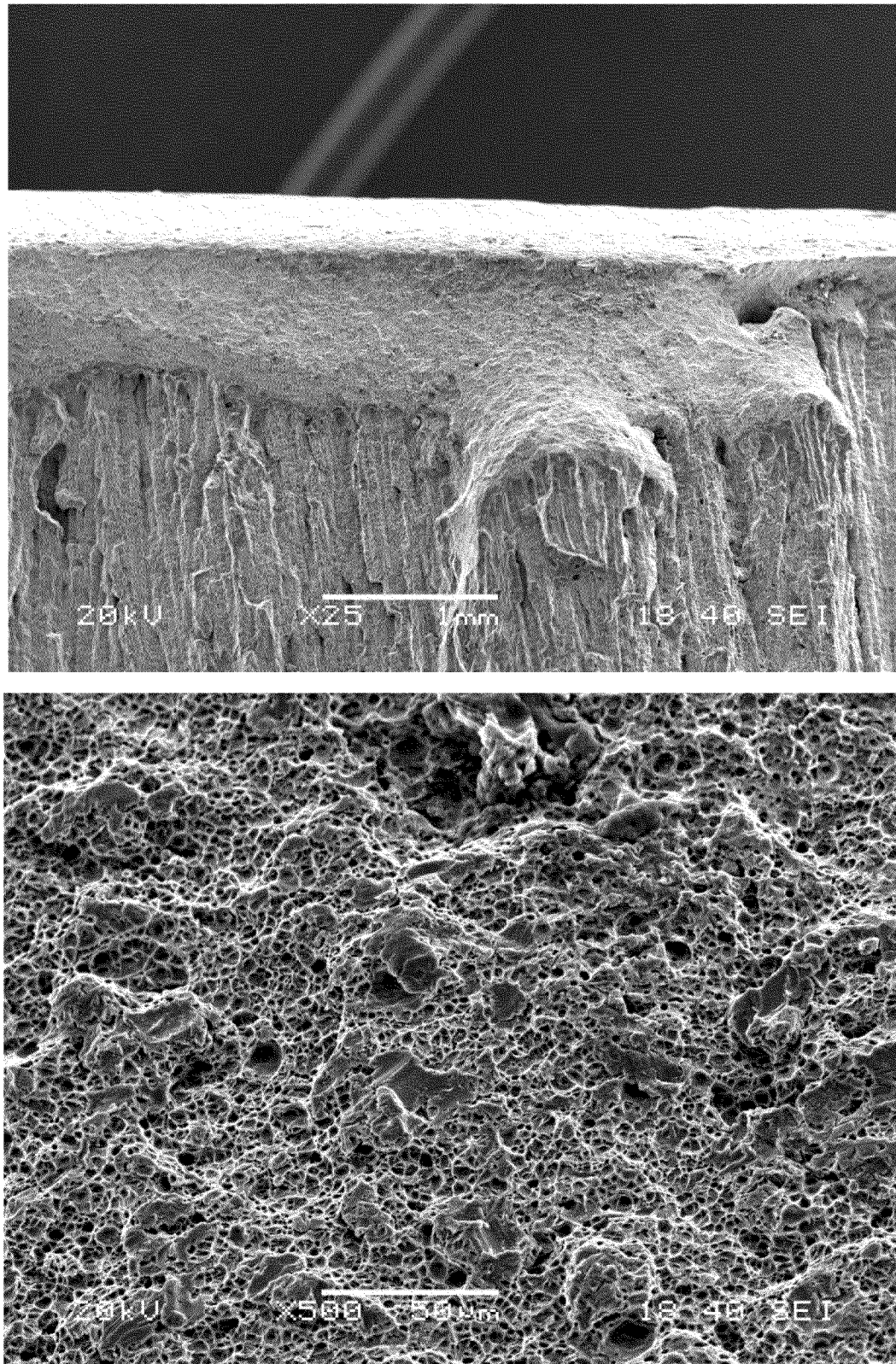


Figure 13. SEM images that show microvoid coalescence above the solidification-cracking zone at the pipe OD.

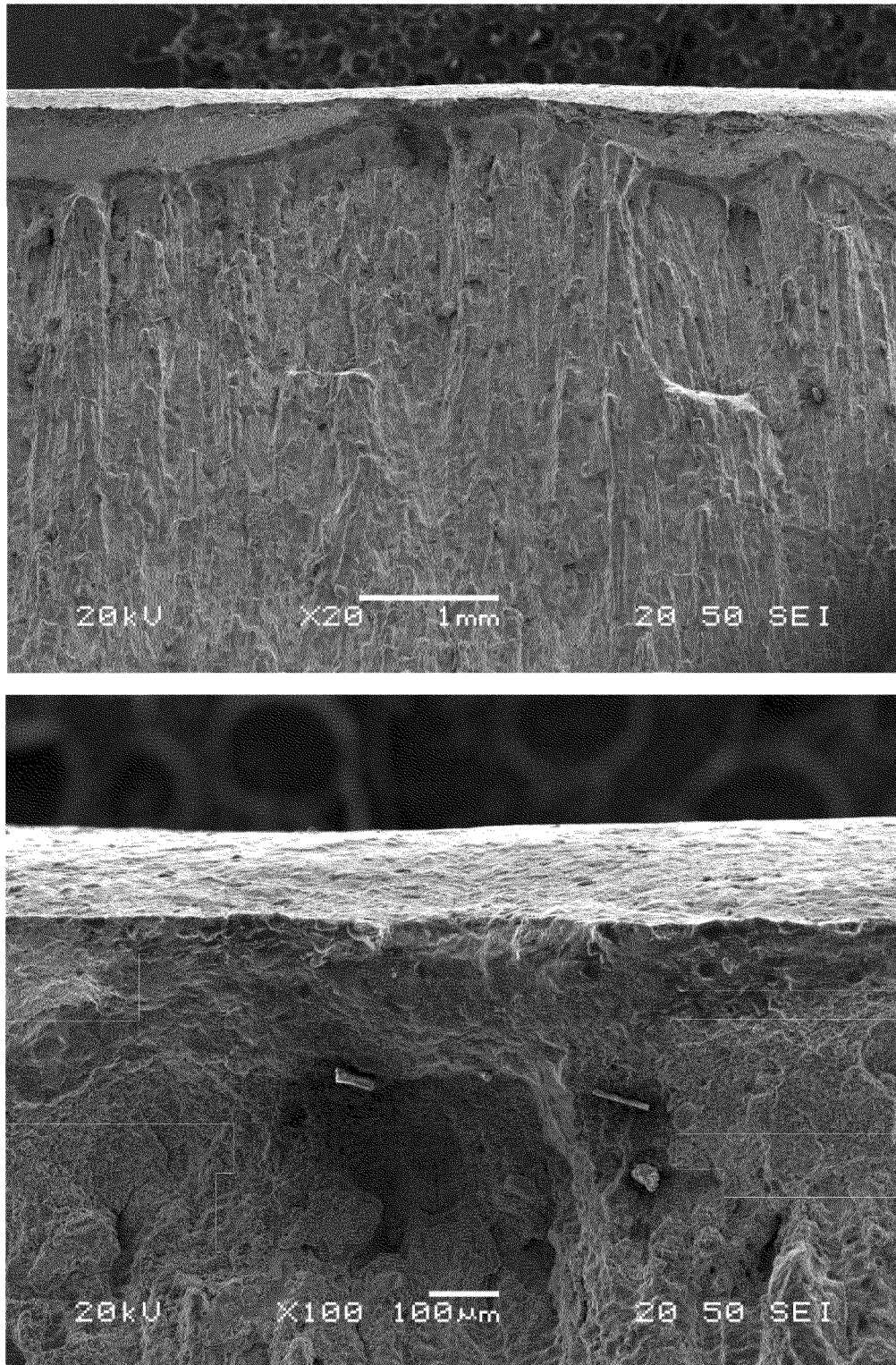


Figure 14. SEM images that show a small portion of the solidification-cracking region, approximately one-millimeter in length, that may have contacted the outside surface of the weld.

Metallographic Examination

Metallographic specimens were removed from the rupture area, as well as from portions of the intact seam weld, girth welds, base metal, and discontinuities found during visual and non-destructive inspection. Specimens were matched and removed from both sides of the rupture for metallographic analysis, shown in Figure 15. The rupture faces on these samples were placed together, and the specimens were ground and polished perpendicular to the fracture plane. Low magnification analysis of the cross section indicates that the OD weld was made first, and the ID weld was made second on the subject seam weld. Misalignment between the inner and outer welds was observed, shown in Figure 16. Along with small weld sizes, the misalignment contributed to the observed lack of penetration. The current version of API 5L specifies that the maximum misalignment of the weld beads shall not exceed 3 mm (0.1 inch) for pipe with specified wall thicknesses less than 0.8 inch¹. Metallographic analysis of the base metal indicated a proeutectoid ferrite/pearlite base metal microstructure, typical for API X52 base metal material, shown in Figure 17.

An intact seam weld sample (T117-CC-T-W) was removed from just west of the rupture, shown in Figure 18. A portion of the sample was ground and polished on a plane perpendicular to the length of the weld. Inner and outer weld misalignment and lack-of-penetration was observed, shown in Figure 19. Lack of penetration was observed at the center of the weld, shown in Figure 20, and a relatively small area of solidification cracking was observed within the OD weld, shown in Figure 21.

An intact portion of the factory girth weld just upstream of the fracture origin was also sectioned and removed for metallurgical analysis, shown in Figure 22. The weld was sectioned on a plane parallel to the axis of the pipe to allow inspection transverse to the welding direction (parallel to the longitudinal axis of the pipe). Metallographic analysis indicated that the girth weld was a multi-pass weld.

¹ ANSI/API Specification 5L, "Specification for Line Pipe", 44th Edition, American Petroleum Institute, October 2010.

Weld discontinuities were visually observed along the ID seam weld both east and west of the rupture. These discontinuities were identified and marked for further metallographic analysis; an example is shown in Figure 23. The samples were cross sectioned, ground, and polished to allow metallographic examination on a plane perpendicular to the longitudinal axis of the pipe. Metallographic examination of these ID weld discontinuities confirmed that they were repair welds, as evidenced by extra deposited weld metal along the ID welds; examples are shown in Figure 24. The repair welding process observed on these welds did not affect their structural integrity.

Weld “buttons” were observed on the pipe OD seam, downstream of the rupture site, and were removed for metallographic examination, shown in Figure 25. The buttons were cross sectioned along a plane perpendicular to the pipe axis and prepared using standard metallographic techniques. Metallographic analysis showed no apparent defects associated with these repair welds along the OD seam (Figure 26). Thus, this OD weld-repair process did not reduce the structural integrity of the pipe.

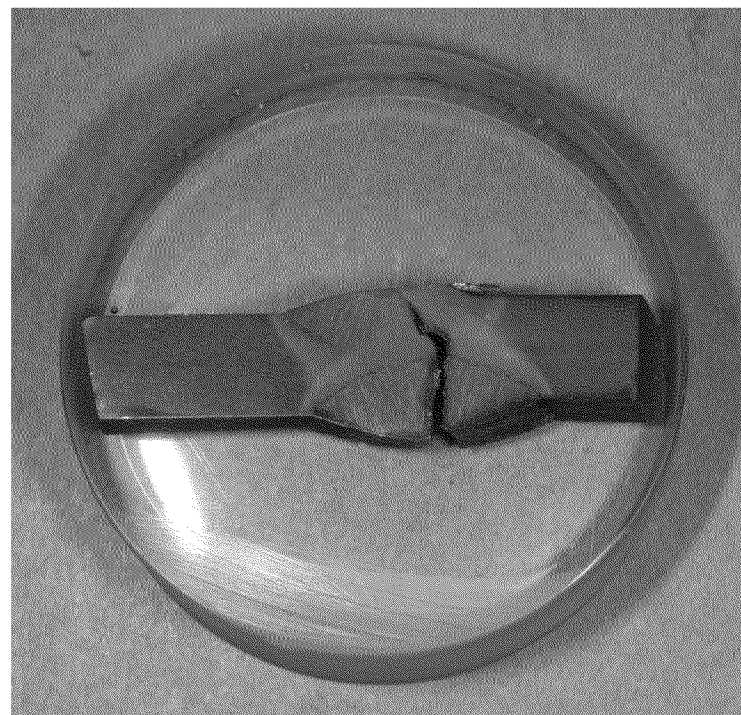
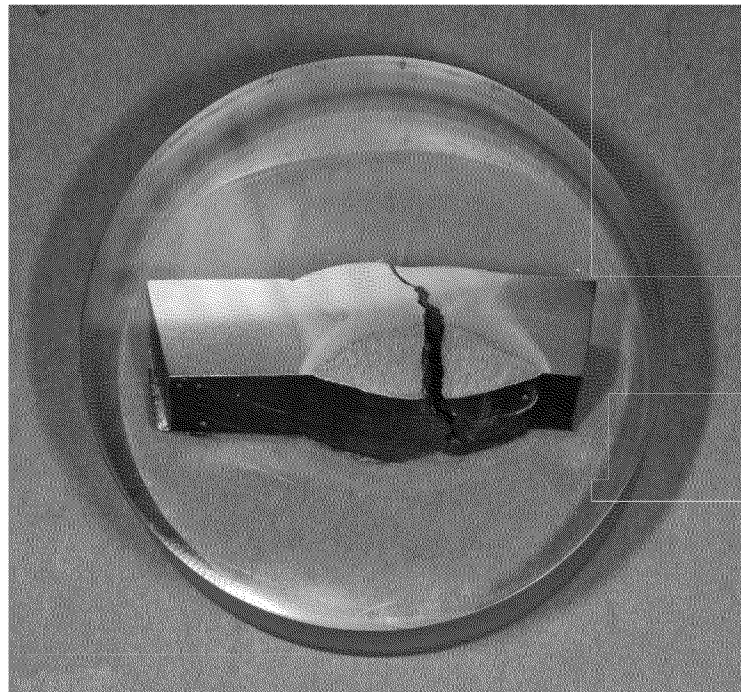


Figure 15. Images that show the metallographic specimens from the rupture area.

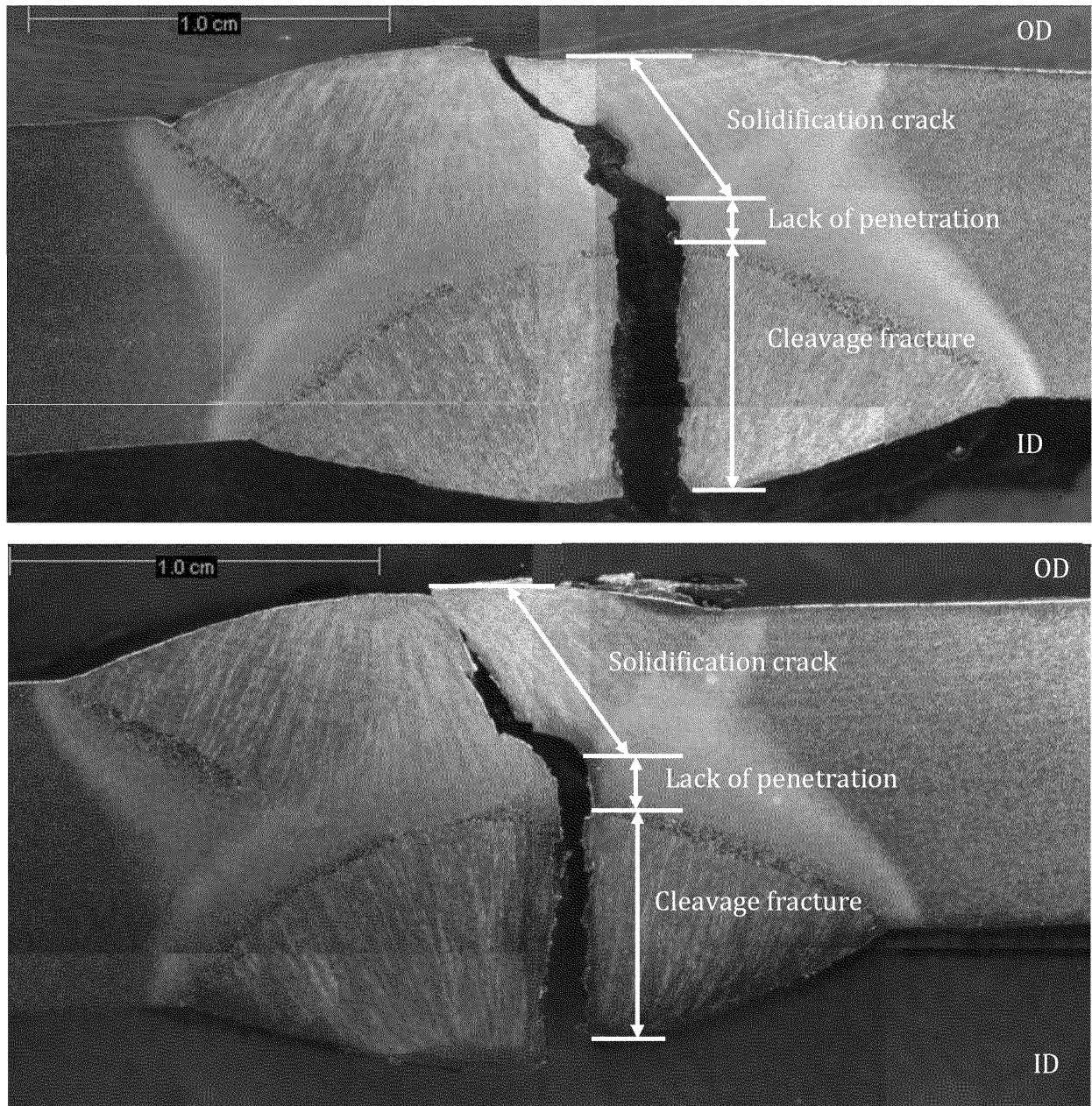


Figure 16. Stereomicroscopic montages of the rupture area metallographic specimens that show weld misalignment.

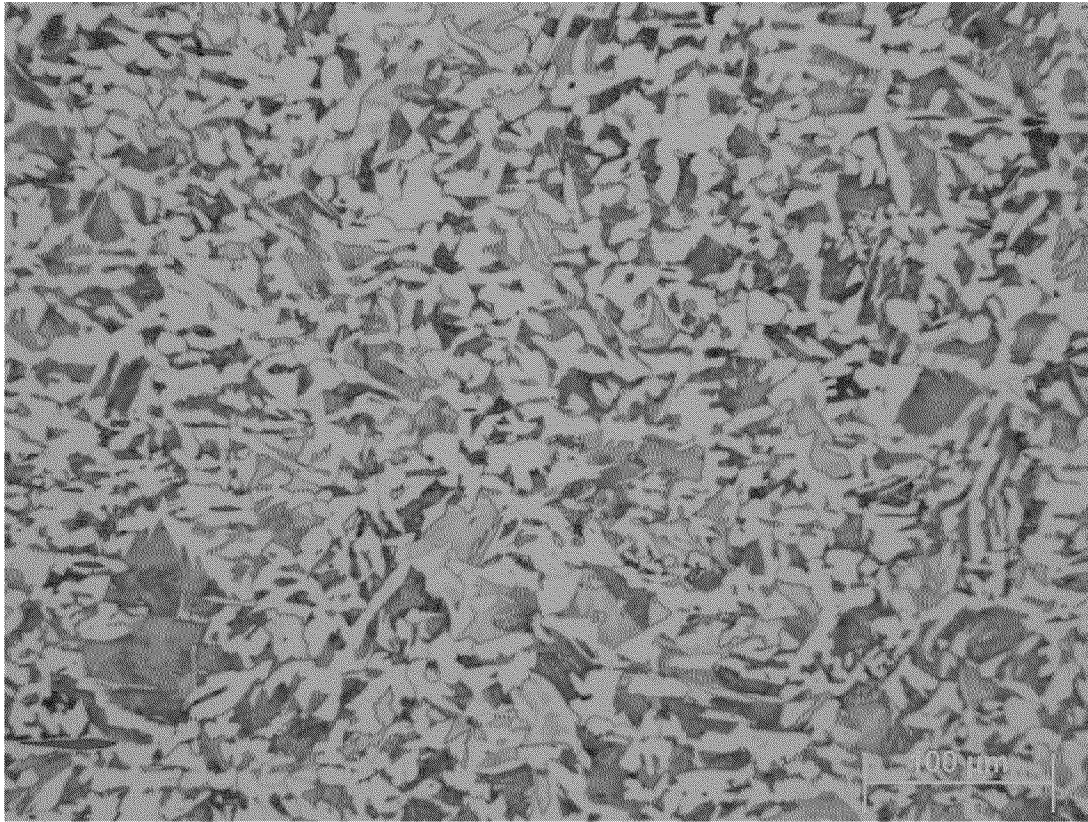


Figure 17. Metallographic image of the subject pipe base metal microstructure.



Figure 18. Images of sample T117-CC-T-W.

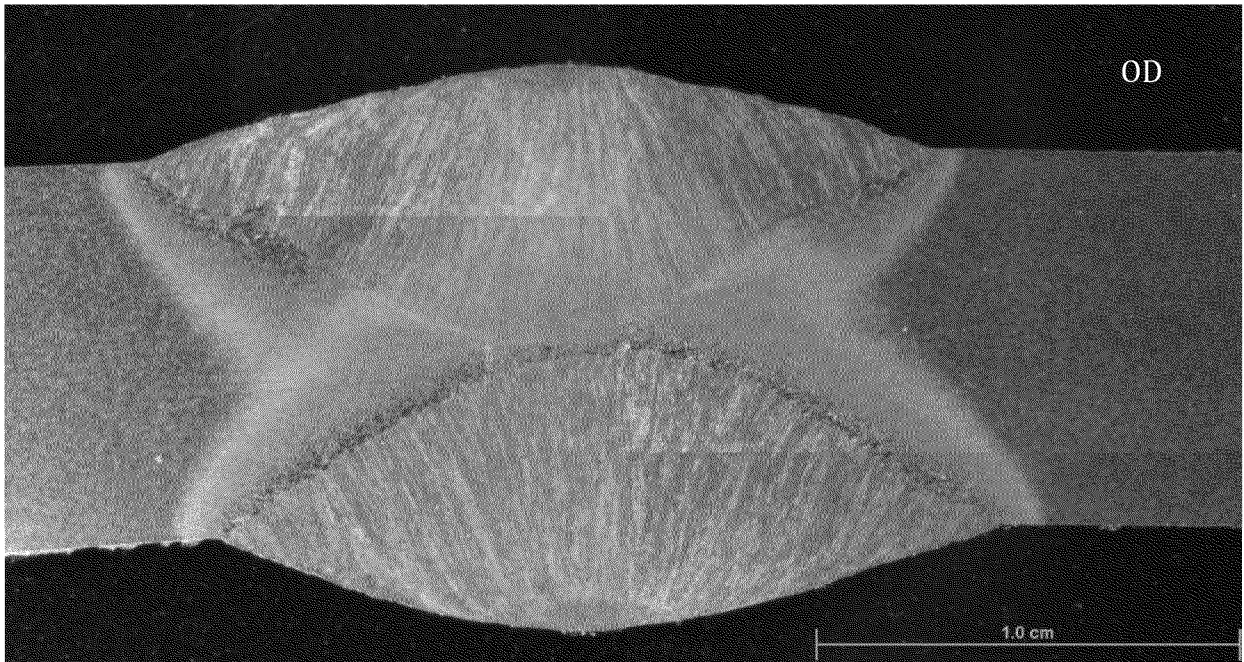


Figure 19. Stereomicroscopic montage that shows the T117-CC-T-W weld seam.

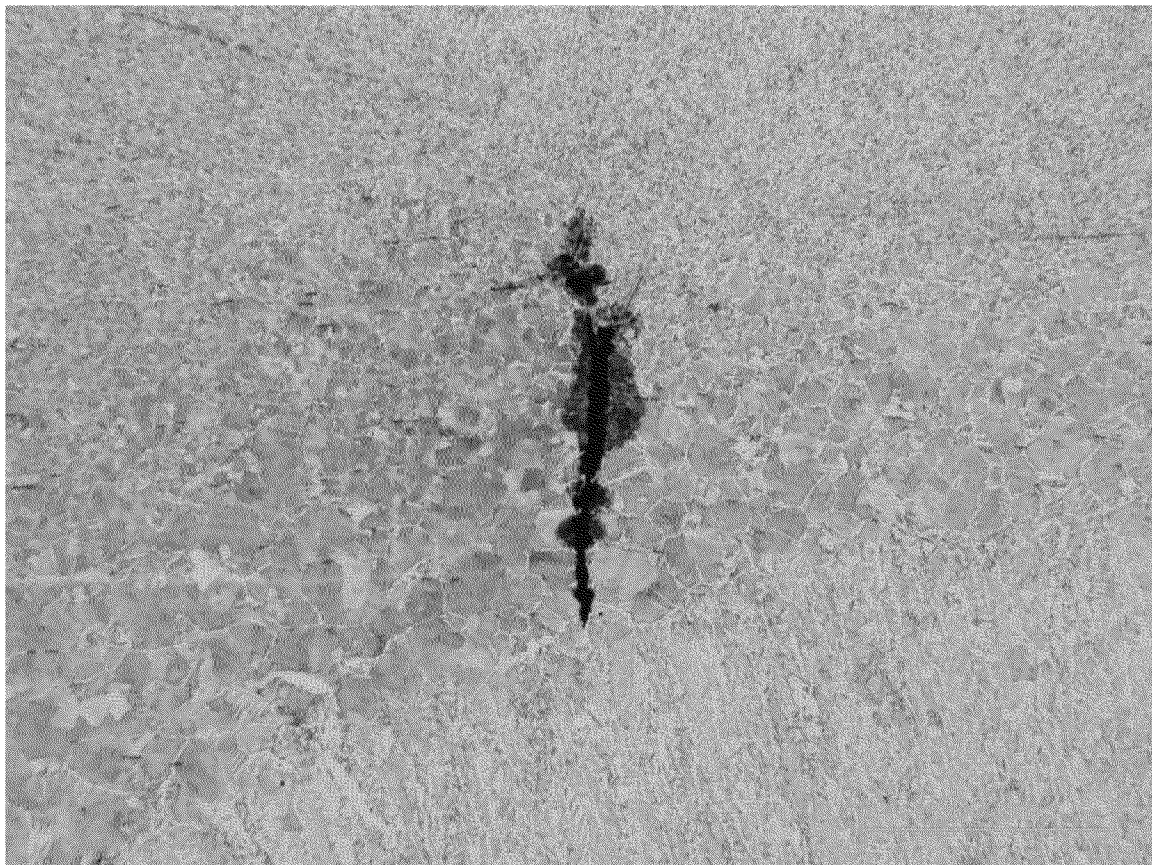


Figure 20. Metallographic image of the lack-of-penetration in Sample T117-CC-T-W.

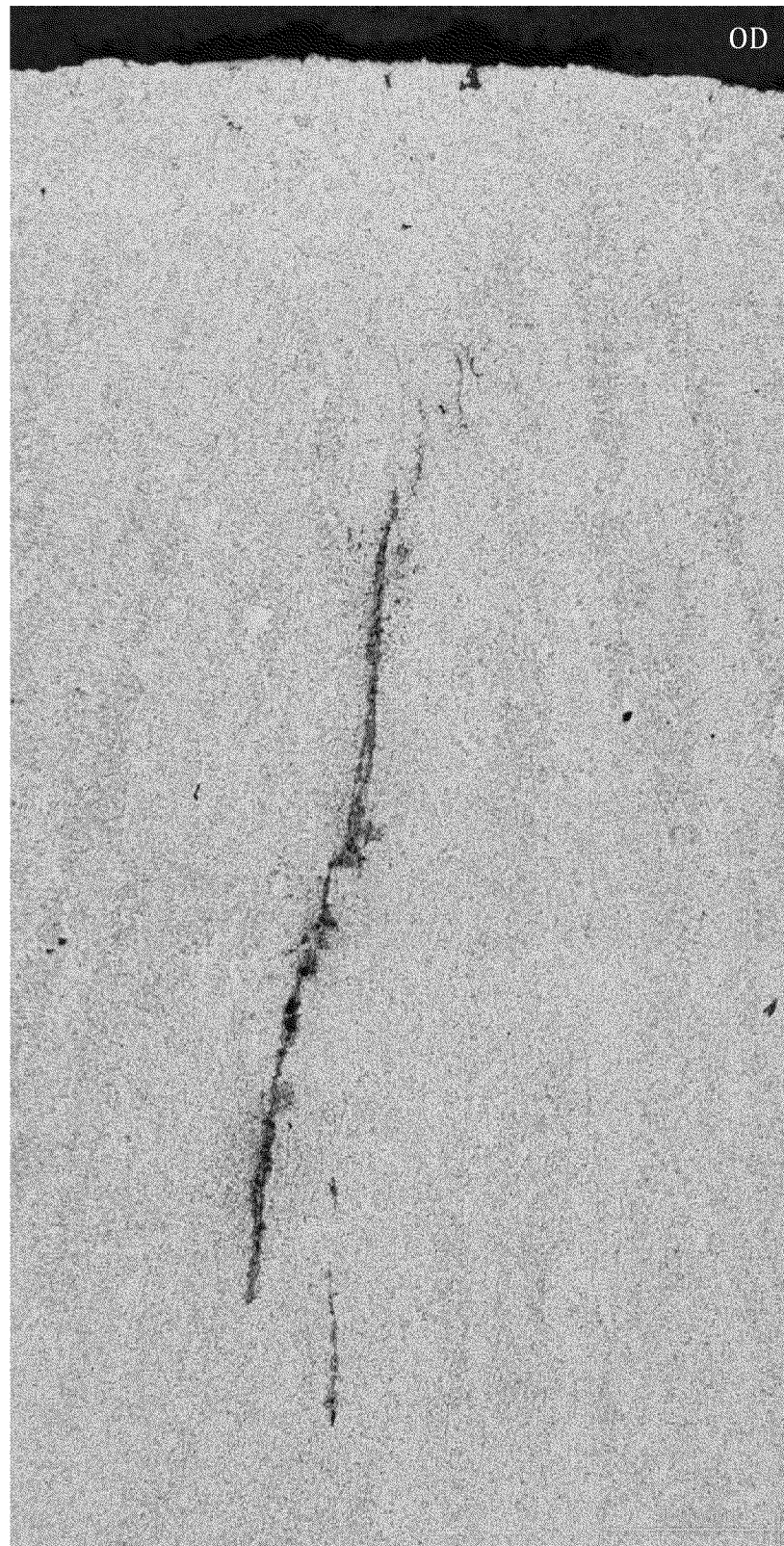


Figure 21. Metallographic montage of OD weld solidification-cracking in Sample T117-CC-T-W.

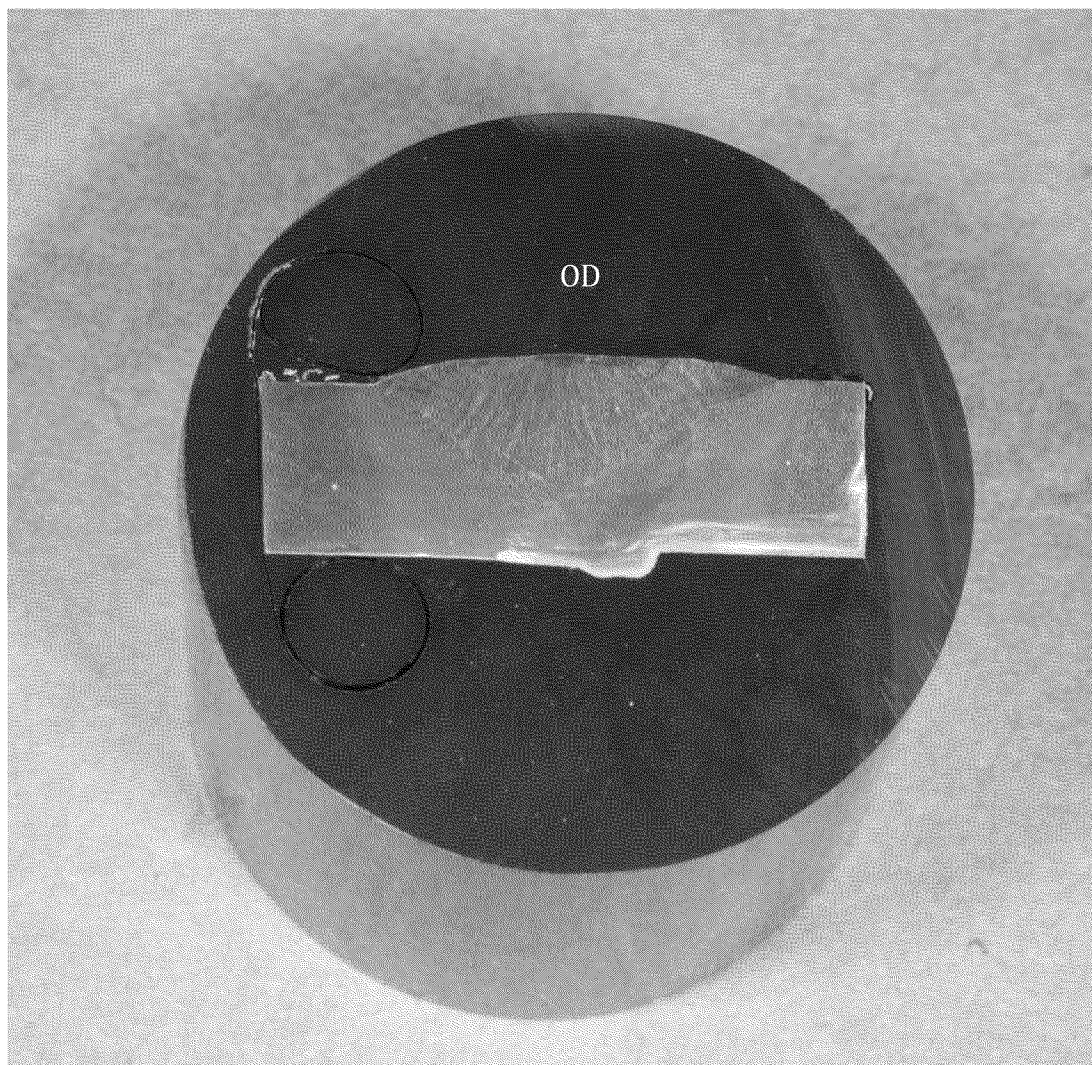
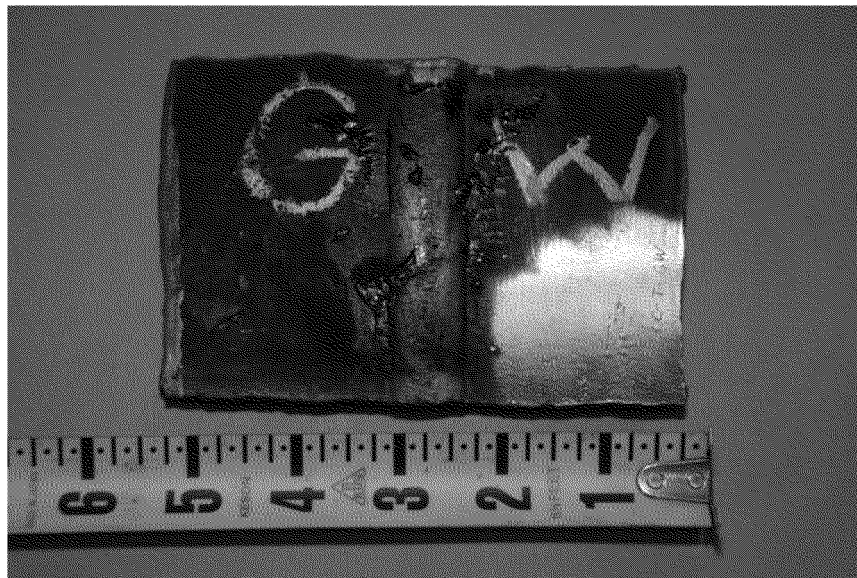


Figure 22. Photographs of factory girth weld.



Figure 23. Images showing an example of a weld discontinuity observed along the ID seam weld.

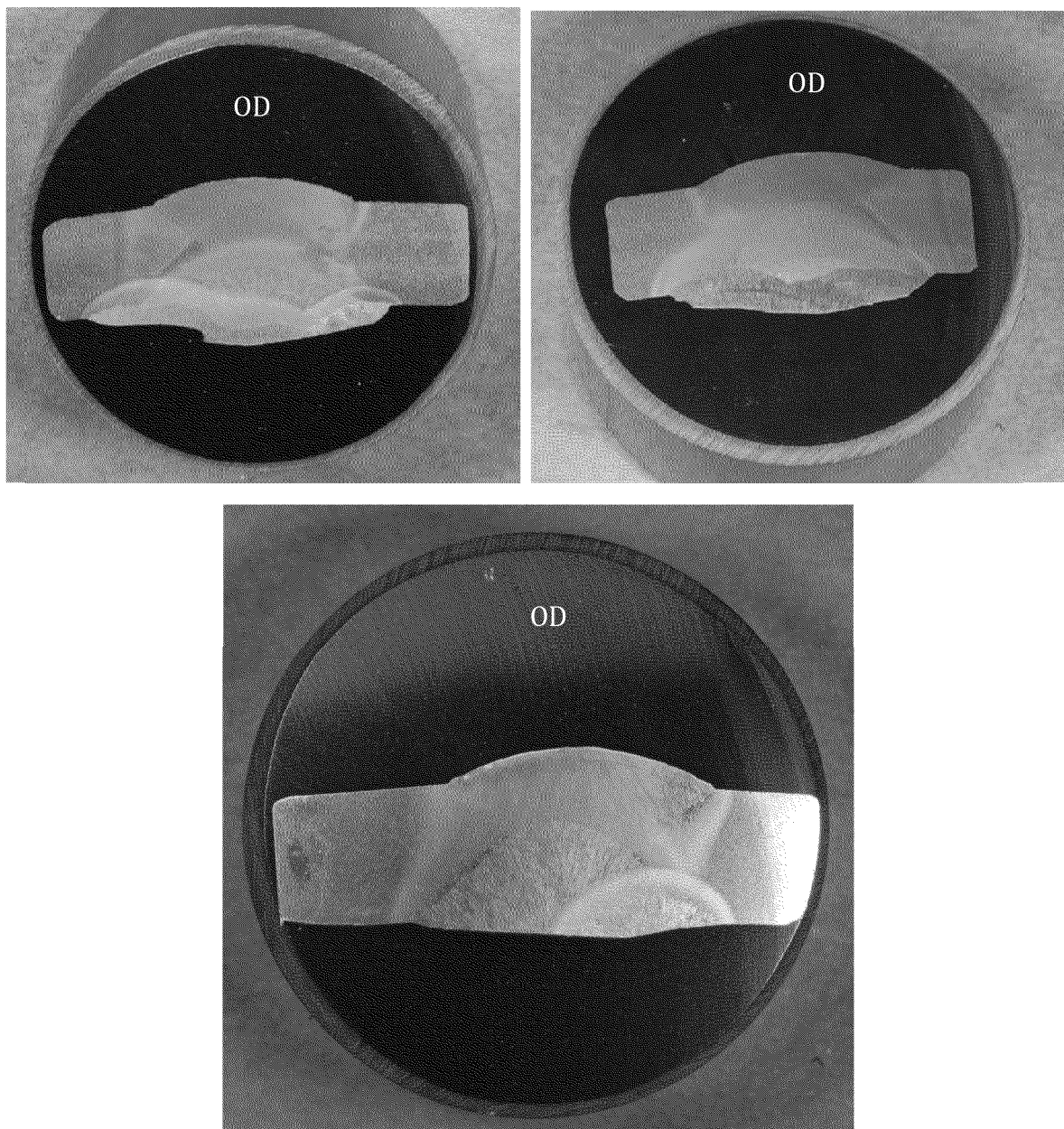


Figure 24. Images of metallographic cross-sections showing ID repair welds.

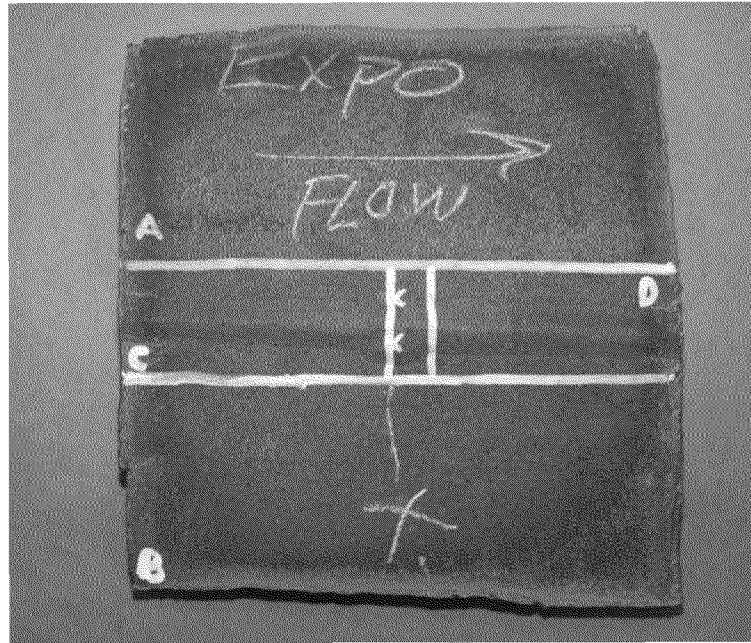


Figure 25 Window that contains specimen marking and the two OD “button” welds.

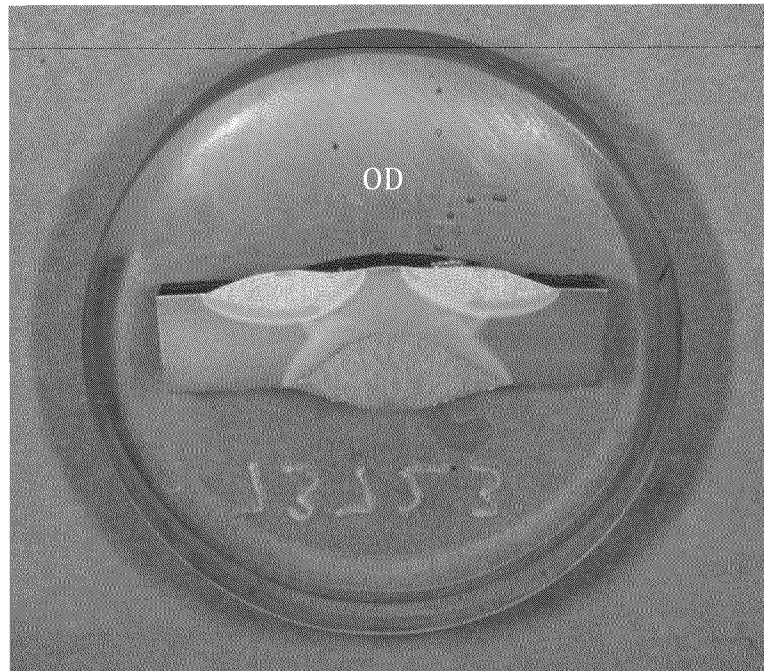


Figure 26 Photograph of OD weld button metallographic mount.

Mechanical Testing

Mechanical testing was conducted at Anamet Inc. to compare base and weld metal properties from the subject pipe with API 5L specifications. Anamet's reports are provided in Appendix A of this report. Tensile test specimens were removed from eight pipe locations. Tensile test results indicate that all samples removed from the piping met API 5L specifications for tensile properties. The elongation for the four base metal samples tested exceeded the current API 5L specifications for API X52 grade steel given sample dimensions. Elongation specifications are not required for weld metal samples.

Table 1. ASTM A370-10 tensile test results

Specimen ID	Weld or Base Metal Specimen	Tensile Strength (ksi)	Yield Strength 0.5% EUL (ksi)	Elongation in 2-inches (%)	Fracture Location
T-117-CE-LS-W-E-1	weld	90.2	73.9	20	Base Metal
T-117-CE-LS-W-B	base metal	85.4	65.5	31	n/a
T-117-CW-LS	weld	91.6	76.8	12.5	Weld
T-117-CW-B	base metal	86.5	67.7	31	n/a
T-117-1-E-LS	weld	88.8	69.3	20.5	Base Metal
T-117-1-E-BM	base metal	85.6	67.8	30.5	n/a
T-117-2-W-LS	weld	89.0	71.6	18.5	Base Metal
T-117-2-W-BM	base metal	88.3	66.0	29.5	n/a
API 5L (2010) X52 Specification		66.7	52.2	24.5*	

* Note that the specified elongation is a function of the tensile specimen cross-sectional area, which varies slightly between samples.

Charpy V-notch (CVN) testing was conducted at a temperature range of -30°F to 100°F. Samples for CVN testing were removed from eight pipe locations. Percent shear values indicate that upper-shelf toughness behavior was likely not achieved. CVN performance specifications were not required for API X52 piping from the 1950's.

Table 2. T-117-CE-LS-W-E ASTM A370-10 Charpy V-notch impact test results

Temperature	Energy Absorbed (ft-lb)	Lateral Expansion (mils)	Shear (%)
-30°F	7.5	11	45
	4	6	30
0°F	10	15	55
	9.5	17	50
+32°F	13.5	19	41
	16.5	23	50
	13	21	42
+40°F	14	20	50
	13.5	21	29
+50°F	10.5	17	37
	15	22	37
	16	24	38
+70°F	19	28	59
	21	32	50
+100°F	24	32	61
	20	29	50

Table 3. T-117-CE-LS-W-B ASTM A370-10 Charpy V-notch impact test results

Temperature	Energy Absorbed (ft-lb)	Lateral Expansion (mils)	Shear (%)
-30°F	3	3	< 3
	2.5	1	< 3
0°F	7	11	9
	8.5	10	9
+32°F	11	15	18
	10.5	15	9
	10.5	16	14
+40°F	5.5	10	29
	12.5	18	25
+50°F	12.5	19	33
	12	19	29
	12	18	29
+70°F	16	24	43
	15.5	23	33
+100°F	19	28	47
	20.5	31	64

Table 4. T-117-CW-LS ASTM A370-10 Charpy V-notch impact test results

Temperature	Energy Absorbed (ft-lb)	Lateral Expansion (mils)	Shear (%)
-30°F	5	6	55
	5	8	55
0°F	5.5	8	37
	13	19	46
+32°F	11	19	55
	11	18	48
	16.5	28	59
+40°F	9	16	55
	15	22	50
+50°F	16	22	59
	11	18	53
	17.5	25	61
+70°F	16.5	23	41
	19	26	41
+100°F	24	32	57
	21	29	57

Table 5. T-117-CW-B ASTM A370-10 Charpy V-notch impact test results

Temperature	Energy Absorbed (ft-lb)	Lateral Expansion (mils)	Shear (%)
-30°F	5.5	6	< 3
	5	6	< 3
0°F	8.5	10	< 3
	8	10	< 3
+32°F	11	17	28
	10	15	18
	11	16	25
+40°F	12.5	18	25
	13	20	30
+50°F	14	22	23
	13.5	21	29
	11	19	29
+70°F	17	26	43
	17	25	46
+100°F	24	36	68
	22	33	64

Table 6. T-117-1-E-LS ASTM A370-10 Charpy V-notch impact test results

Temperature	Energy Absorbed (ft-lb)	Lateral Expansion (mils)	Shear (%)
+32°F	9	14	23
	7.5	15	37
	8	13	32
+50°F	9.8	20	46
	8.5	16	37
	9.5	18	32

Table 7. T-117-1-E-BM ASTM A370-10 Charpy V-notch impact test results

Temperature	Energy Absorbed (ft-lb)	Lateral Expansion (mils)	Shear (%)
+32°F	11.5	18	23
	9.5	16	18
	11	17	25
+50°F	14.5	24	40
	13	19	34
	15	25	38

Table 8. T-117-2-W-LS ASTM A370-10 Charpy V-notch impact test results

Temperature	Energy Absorbed (ft-lb)	Lateral Expansion (mils)	Shear (%)
+32°F	7	11	42
	7	11	47
	9	16	18
+50°F	9	13	25
	12	17	42
	12	18	28

Table 9. T-117-2-W-BM ASTM A370-10 Charpy V-notch impact test results

Temperature	Energy Absorbed (ft-lb)	Lateral Expansion (mils)	Shear (%)
+32°F	13.5	17	18
	9	14	18
	10.5	15	23
+50°F	14	20	32
	13.5	19	32
	17	23	28

Chemical Analysis

Specimens for chemical analysis were removed from four pipe base metal locations, and tested to compare the subject pipe elemental compositions with API specifications for X52. The results indicate that three of the four pipe test sample chemistries exceeded current API X52 requirements for carbon and sulfur. Allowable chemistries were not required for X52 grade pipe steel in 1950. However, the subject base metal specimens met the most stringent 1949 API 5LX specifications for X42 grade material (0.33 % C, 1.28% Mn, 0.055% P, 0.065% S).

Table 10. Quantitative chemical analysis test results

Element	T-117-CE-LS-W-B (weight %)	T-117-CW-B (weight %)	T-117-1-E-BM (weight %)	T-117-2-W-BM (weight %)	API 5L (2010) X52 Spec. (wt. %)
Carbon	0.28	0.29	0.29	0.30	0.28 max
Chromium	0.02	0.01	0.01	0.03	
Niobium	<0.005	<0.005	<0.005	<0.005	
Copper	0.07	0.08	0.08	0.09	
Iron	Main Constituent	Main Constituent	Main Constituent	Main Constituent	
Manganese	0.95	1.02	1.02	1.03	1.40 max
Molybdenum	<0.005	<0.005	<0.005	<0.005	
Nickel	0.06	0.08	0.08	0.08	
Phosphorus	0.011	0.012	0.012	0.023	0.030 max
Silicon	0.05	0.07	0.07	0.06	
Sulfur	0.027	0.055	0.055	0.040	0.030 max
Titanium	<0.005	<0.005	<0.005	<0.005	
Vanadium	<0.005	<0.005	<0.005	0.30	Sum of Ti, Nb, V < 0.15%

Discussion and Conclusions

Our metallurgical analysis indicates that the Line 300B hydrotest failure was caused by the existence of solidification cracking in the outer submerged-arc weld combined with lack-of-penetration between the OD and ID welds.

Solidification cracking (also referred to as hot cracking) can occur in carbon and low-alloy steel welds when the solidifying metal cannot support the thermally or mechanically-induced strain from the welding process. The cracks typically follow the weld centerline, do not always come to the surface, and are typically heavily oxidized,² consistent with the discontinuity observed in the Line 300B hydrotest rupture. Interdendritic segregation of impurity elements such as sulfur and phosphorus (as well as carbon, nickel, niobium, and boron) contribute to solidification cracking. High sulfur content is one of the most common causes of solidification cracking in welded steels.³ In submerged arc-welds, bead shape, joint restraint, pre-heat temperatures, and correct electrode and flux combinations can affect susceptibility to solidification cracking.⁴ Carbon and sulfur content above current specified maximum levels for X52 was noted for three of the four specimens tested from the Line 300B pipe. Due to the relative proximity to the factory girth weld and associated “squirt” welds, the solidification cracking in the L-300B hydrotest failure may have been associated with cracking from poor mechanical restraint common at joint ends in early 1950-era double submerged arc-welds.⁵

The subject seam-weld rupture also exhibited un-fused material at the center of the weld, caused by lack-of-penetration between the inner and outer welds. Lack-of-penetration occurs in DSAW pipe when the weld metal from inner and outer welds does not intersect. In this case, small welds, as well as misalignment between the inner and outer welds, resulted in the lack-of-penetration. The lack-of-penetration contributed to the hydrotest failure.

² ASM Handbook, Volume 6: Welding, Brazing, and Soldering, ASM International, 2003, pp. 649-651.

³ Welding Handbook, Volume 4: Materials and Applications Part 2, Eighth Edition, American Welding Society, 1998, p. 10.

⁴ ASM Specialty Handbook, Carbon and Alloy Steels, ASM International, 1996, pp.121-122.

⁵ J.F. Kiefner, E.B. Clark, “History of Line Pipe Manufacturing in North America”, ASME, CRTD Vol. 43, 1996.

The solidification cracking and lack-of-penetration existed in the subject pipe from initial fabrication to the final rupture during hydrotesting. Detailed SEM analysis indicated that no progressive crack growth, such as fatigue or SCC, occurred during the life of the pipe/discontinuity. Thus, neither the solidification-crack zone nor the lack-of-penetration grew during service. Further, the subject pipe must not have ever been subjected to a pressure greater than 998 psig in an unconstrained condition (such as during hydrotesting or mill testing) prior to the hydrotest failure.

Metallographic examination of seam weld anomalies found during visual inspection indicated that repairs had been made along the submerged-arc weld. These weld repairs were relatively minor, did not leave large discontinuities, and did not affect the integrity of the pipe.

Limitations

At the request of PG&E, Exponent has conducted an investigation of the rupture that occurred in Line 300B during hydrotesting. Exponent investigated specific issues relevant to this rupture, as requested by the client. The scope of services performed during this investigation may not adequately address the needs of other users of this report, and any re-use of this report or its findings, conclusions, or recommendations presented herein are at the sole risk of the user. The opinions and comments formulated during this assessment are based on observations and information available at the time of the investigation. No guarantee or warranty as to future life or performance of any reviewed condition is expressed or implied.

The findings presented herein are made to a reasonable degree of engineering certainty. We have made every effort to accurately and completely investigate all areas of concern identified during our investigation. If new data becomes available or there are perceived omissions or misstatements in this report regarding any aspect of those conditions, we ask that they be brought to our attention as soon as possible so that we have the opportunity to fully address them.

March 15, 2012

Appendix A

Anamet Inc. Reports



Report No. 5004.6986 Rev. A

February 29, 2012

**MECHANICAL TESTING AND CHEMICAL ANALYSIS OF FIVE PIPE
SECTIONS FROM LINE 300B MP 285 HYDRO TEST FAILURE**

Customer Authorization: CWA # 2500614190

Report To: Pacific Gas and Electric
ATTN: Dave Aguiar
375 North Wiget Lane, Suite 250
Walnut Creek, CA 94958

REPORT

Five pipe sections from Pacific Gas and Electric, Walnut Creek, CA were submitted for mechanical testing and chemical analysis. The samples were from “Line 300B MP 285 Hydro Test Failure”. The samples were identified by PG&E as: T-117-CE-LS-W-E, T-117-CE-LS-W-E-1, T-117-CE-LS-W-B, T-117-CW-LS, and T-117-CW-B. Photographs of the samples as received are shown in Figure 1 through Figure 5.

Tensile testing was conducted on the longitudinal seam weld of T-117-CE-LS-W-E-1 and T-117-CW-LS and the base metal of T-117-CE-LS-W-B and T-117-CW-B. All of the tensile testing was conducted per API 5L¹. The tensile test specimens were oriented in the circumferential direction. The results of the tensile tests are listed in Table 1.

Charpy V-notch impact testing was conducted on the longitudinal seam weld of T-117-CE-LS-W-E and T-117-CW-LS and the base metal of T-117-CE-LS-W-B and T-117-CW-B. The charpy V-notch impact specimens were oriented in the circumferential direction with the notch in the axial direction. The dimensions of all of the charpy V-notch impact specimens was 8.0 mm x 10 mm x 55 mm (thickness x width x length). The results of the charpy V-notch impact tests are listed in Table 2 through Table 5.

Quantitative chemical analysis was completed on the base metal from samples T-117-CE-LS-W-B and T-117-CW-B. The results of the chemical analysis are listed in Table 6.

¹ API 5L – *Specification of Line Pipe*, 2007.

This report shall not be reproduced, except in full, without the written approval of Anamet.

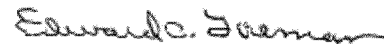
This testing was completed on February 29, 2012 and was performed in accordance with the customer's authorization.

Prepared by:



Ryan Wood
Materials Engineer

Reviewed by:



Edward Foreman
Quality Manager

Table 1
 Results of the Tensile Tests
 (ASTM A 370-10)

	Tensile Strength (ksi)	Yield Strength 0.5% EUL (ksi)	Elongation in 2-inches (%)	Fracture Location
T-117-CE-LS-E-1	90.2	73.9	20	Parent Metal
T-117-CE-LS-W-B	85.4	65.5	31	n/a
T-117-CW-LS	91.6	76.8	12.5	Weld
T-117-CW-B	86.5	67.7	31	n/a

Table 2
 Results of the Charpy V-Notch Impact Tests
 of T-117-CE-LS-W-E
 (ASTM A 370-10)

Temperature	Energy Absorbed (ft lb)	Lateral Expansion (mils)	Shear (%)
-30 °F	7.5	11	45
	4	6	30
0 °F	10	15	55
	9.5	17	50
+32 °F	13.5	19	41
	16.5	23	50
	13	21	42
+40 °F	14	20	50
	13.5	21	29
+50 °F	10.5	17	37
	15	22	37
	16	24	38
+70 °F	19	28	59
	21	32	50
+100 °F	24	32	61
	20	29	50

Table 3
 Results of the Charpy V-Notch Impact Tests
 of T-117-CE-LS-W-B
 (ASTM A 370-10)

Temperature	Energy Absorbed (ft lb)	Lateral Expansion (mils)	Shear (%)
-30 °F	3	3	< 3
	2.5	1	< 3
0 °F	7	11	9
	8.5	10	9
+32 °F	11	15	18
	10.5	15	9
	10.5	16	14
+40 °F	5.5	10	29
	12.5	18	25
+50 °F	12.5	19	33
	12	19	29
	12	18	29
+70 °F	16	24	43
	15.5	23	33
+100 °F	19	28	47
	20.5	31	64

Table 4
 Results of the Charpy V-Notch Impact Tests
 of T-117-CW-LS
 (ASTM A 370-10)

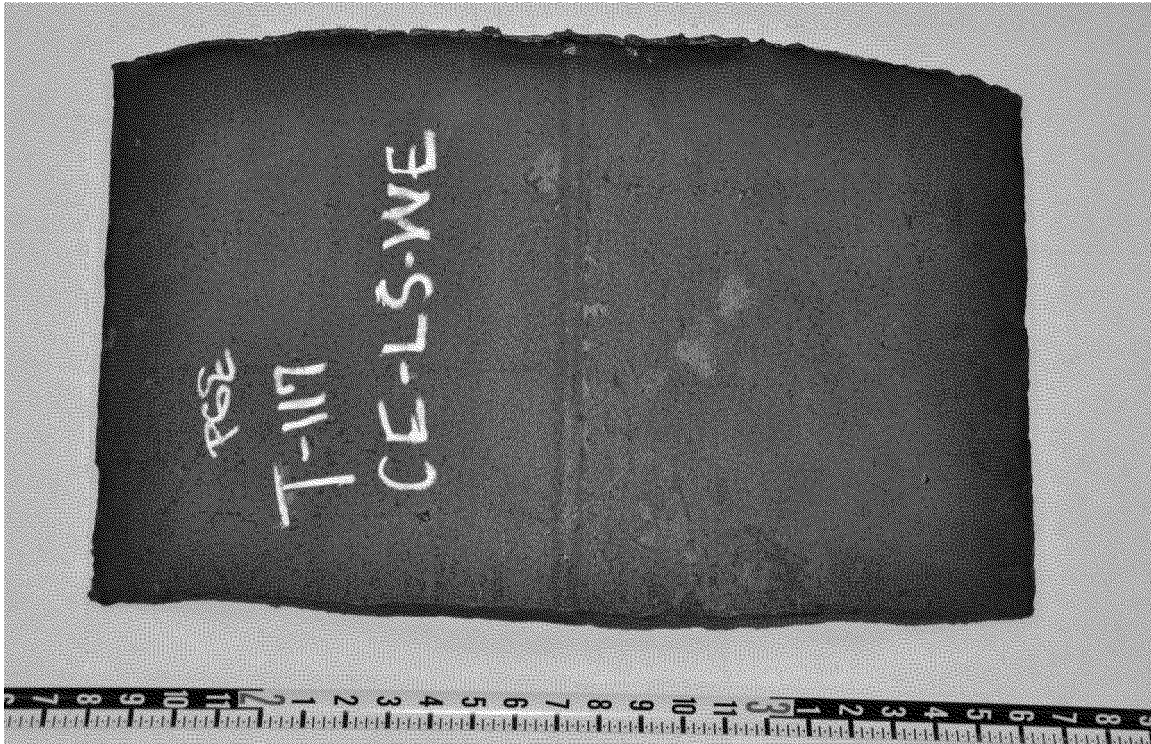
Temperature	Energy Absorbed (ft lb)	Lateral Expansion (mils)	Shear (%)
-30 °F	5	6	55
	5	8	55
0 °F	5.5	8	37
	13	19	46
+32 °F	11	19	55
	11	18	48
	16.5	28	59
+40 °F	9	16	55
	15	22	50
+50 °F	16	22	59
	11	18	53
	17.5	25	61
+70 °F	16.5	23	41
	19	26	41
+100 °F	24	32	57
	21	29	57

Table 5
 Results of the Charpy V-Notch Impact Tests
 of T-117-CW-B
 (ASTM A 370-10)

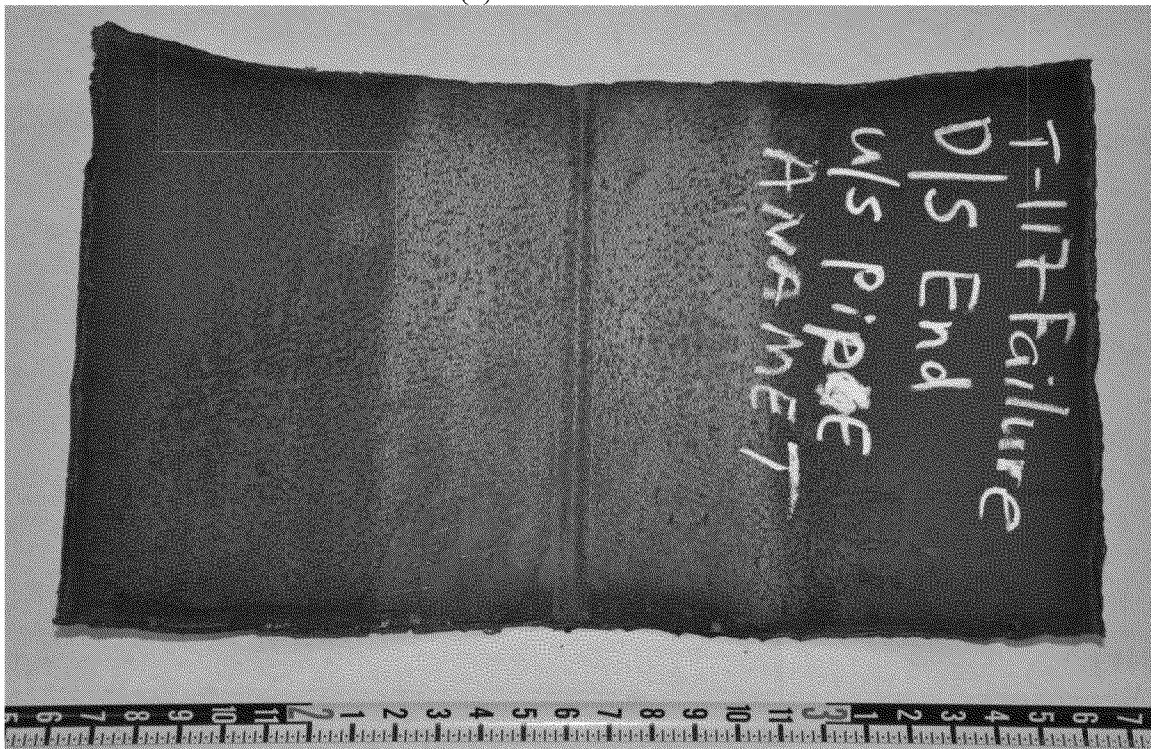
Temperature	Energy Absorbed (ft lb)	Lateral Expansion (mils)	Shear (%)
-30 °F	5.5	6	< 3
	5	6	< 3
0 °F	8.5	10	< 3
	8	10	< 3
+32 °F	11	17	28
	10	15	18
	11	16	25
+40 °F	12.5	18	25
	13	20	30
+50 °F	14	22	23
	13.5	21	29
	11	19	29
+70 °F	17	26	43
	17	25	46
+100 °F	24	36	68
	22	33	64

Table 6
 Results of Quantitative Chemical Analysis of
 T-117-CE-LS-W-B and T-117-CW-B

Element	T-117-CE-LS-W-B (weight %)	T-117-CW-B (weight %)
Carbon (C)	0.28	0.27
Chromium (Cr)	0.02	0.03
Columbium (Cb)	<0.005	<0.005
Copper (Cu)	0.07	0.04
Iron (Fe)	Main Constituent	Main Constituent
Manganese (Mn)	0.95	0.93
Molybdenum (Mo)	<0.005	<0.005
Nickel (Ni)	0.06	0.07
Phosphorus (P)	0.011	0.023
Silicon (Si)	0.05	0.07
Sulfur (S)	0.027	0.025
Titanium (Ti)	<0.005	<0.005
Vanadium (V)	<0.005	<0.005



(a) Outside surface

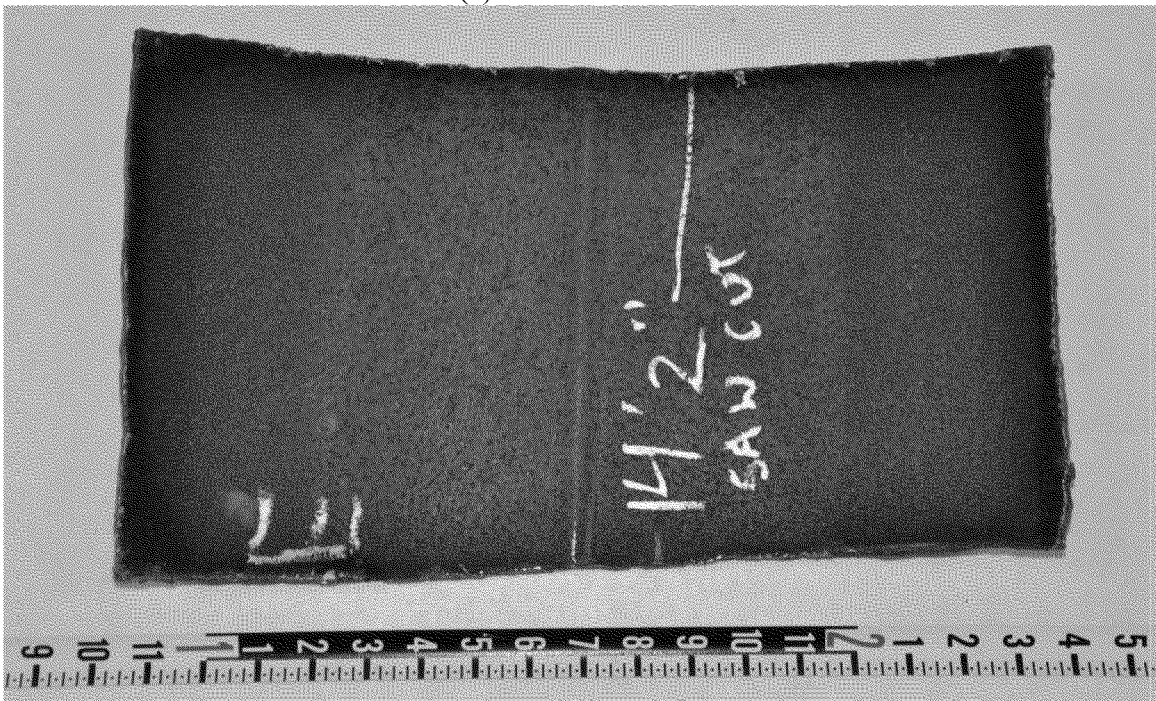


(b) Inside surface

Figure 1 Photographs of T-117-CE-LS-W-E as-received



(a) Outside surface

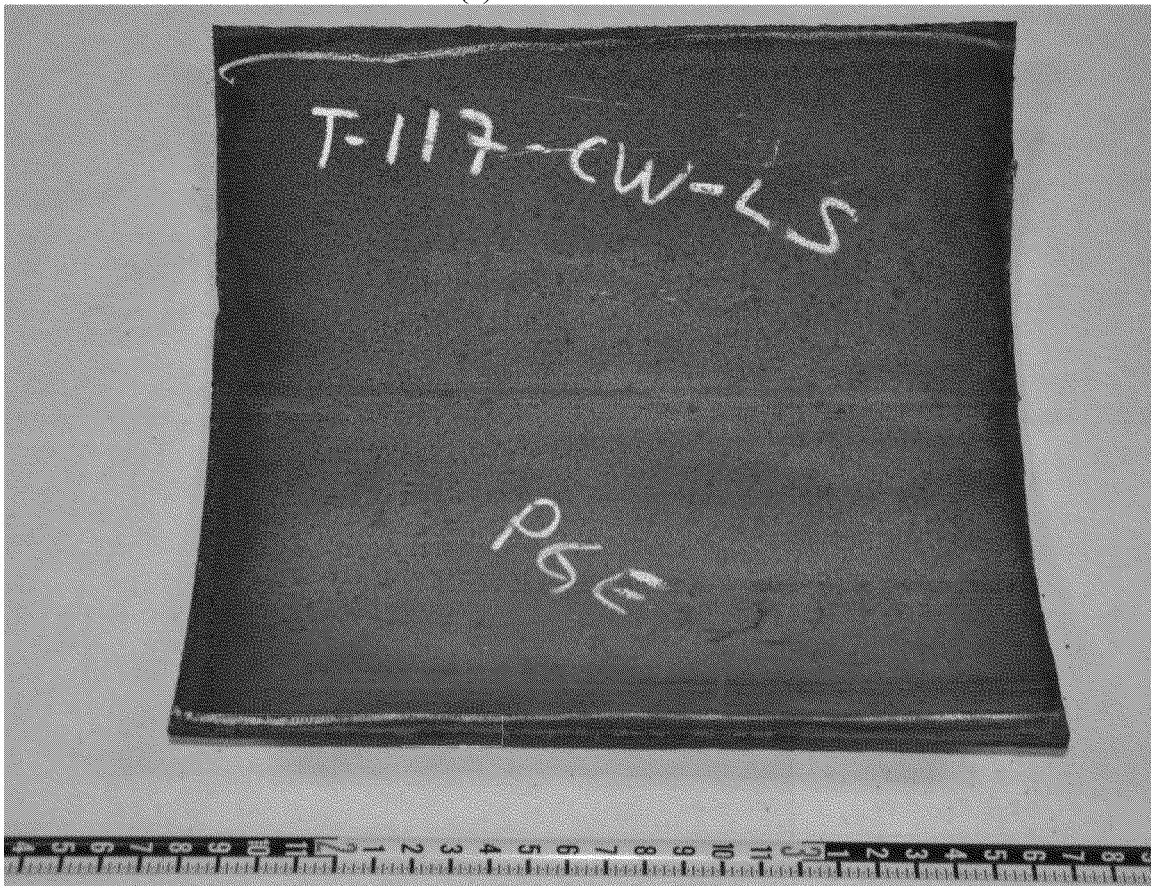


(b) Inside surface

Figure 2 Photographs of T-117-CE-LS-W-E-1 as-received.

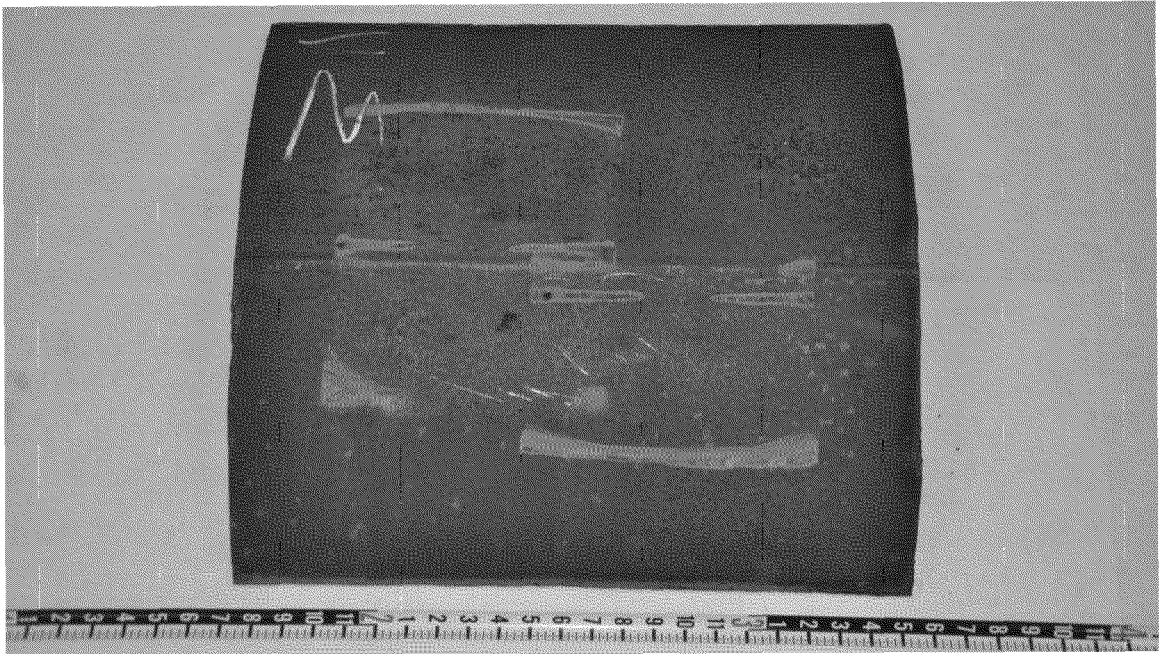


(a) Outside surface

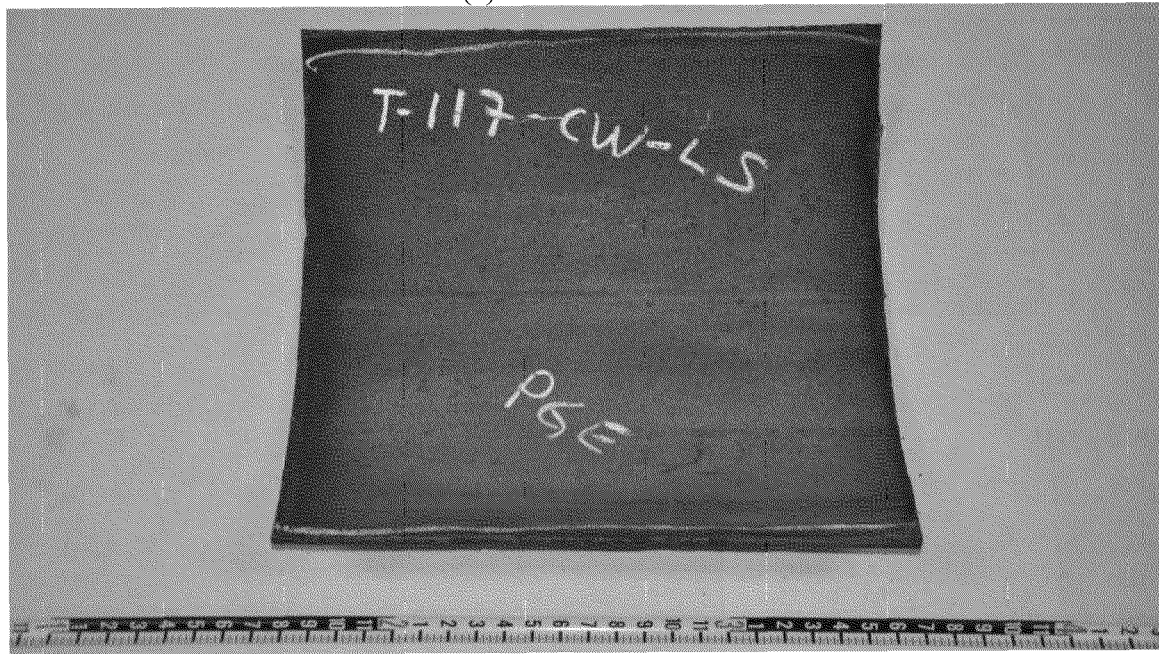


(b) Inside surface

Figure 3 Photographs of T-117-CE-LS-W-B as-received.

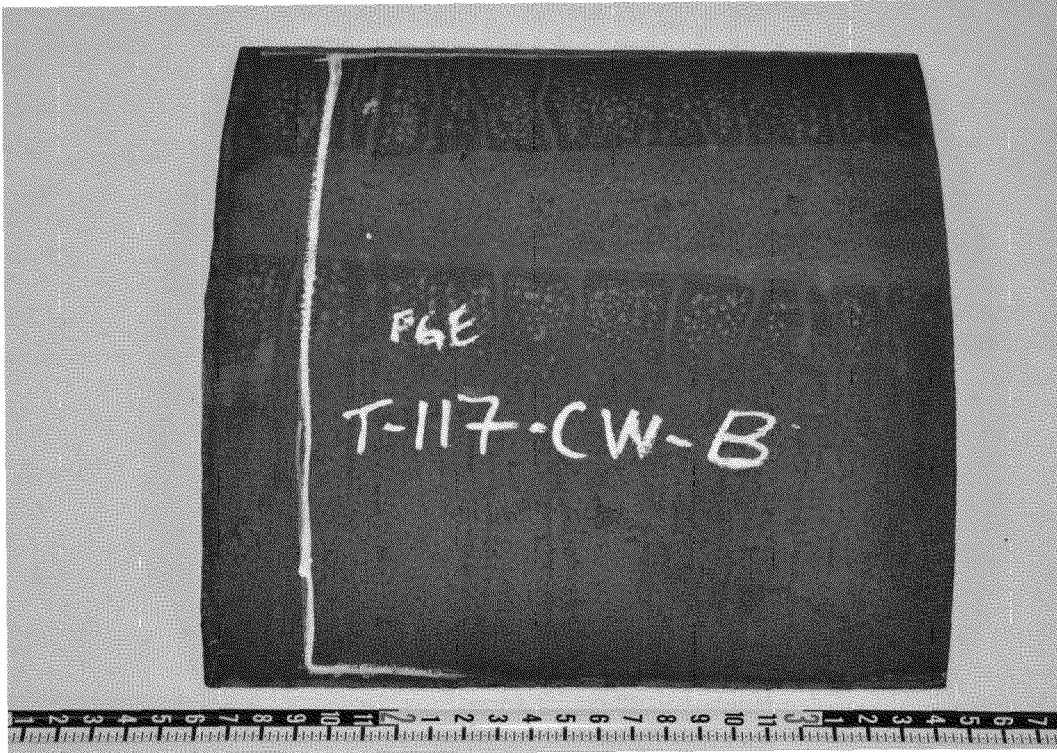


(a) Outside surface

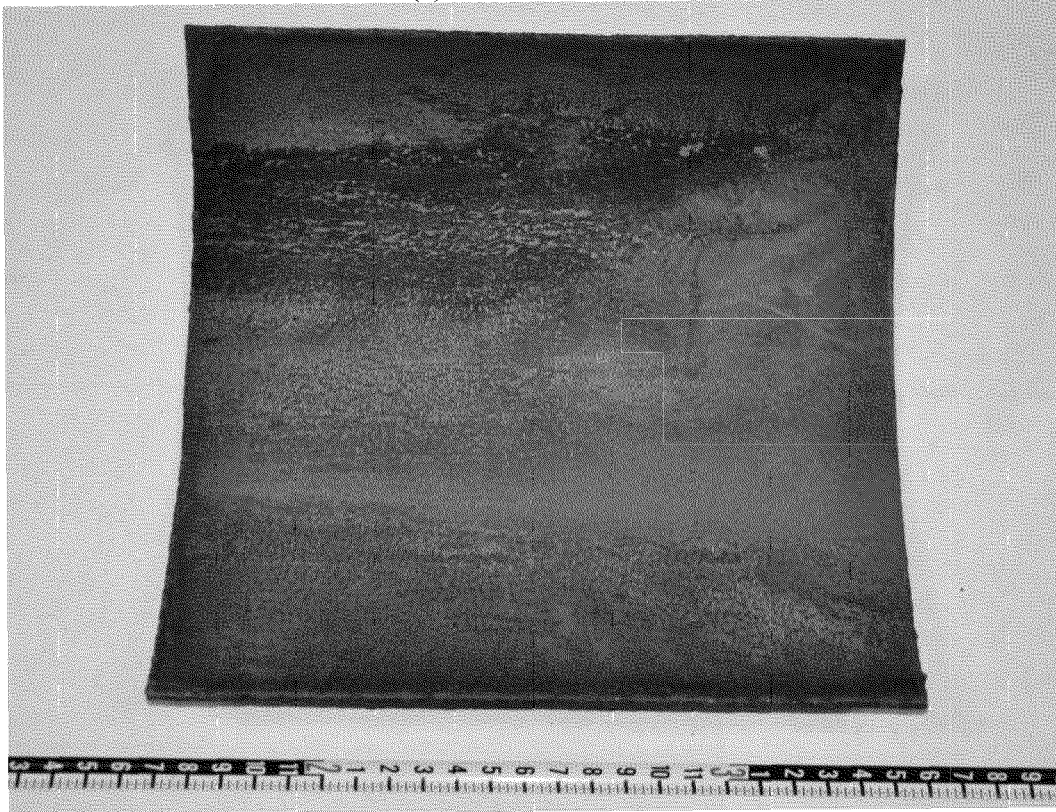


(b) Inside surface

Figure 4 Photographs of T-117-CW-LS as-received.



(a) Outside surface



(b) Inside surface

Figure 5 Photographs of T-117-CW-B as-received.

Appendix A – Parts List and Preservation

Table 1a*
 Parts List for T-117-CE-LS-W-E

Identification	Description
T-117-CE-LS-W-E-A	Remnant
T-117-CE-LS-W-E-A-1	Remnant
T-117-CE-LS-E-W-B-1	Remnant
T-117-CE-LS-E-W-B-2	Charpy V-notch impact specimens (16 total)
T-117-CE-LS-E-W-B-3	Remnant
T-117-CE-LS-E-W-B-4	Remnant
T-117-CE-LS-E-W-B-5	Remnant

*Figure 1a identifies the location of each piece.

Appendix A - Parts List and Preservation

Table 2a*
 Parts List for T-117-CE-LS-W-E-1

Identification	Description
T-117-CE-LS-W-E-1-A	Remnant
T-117-CE-LS-W-E-1-B-1	Remnant
T-117-CE-LS-W-E-1-B-2	Tensile test specimen
T-117-CE-LS-W-E-1-B-3	Remnant
T-117-CE-LS-W-E-1-B-4	Remnant

*Figure 2a identifies the location of each piece.

Appendix A – Parts list and Preservation

Table 3a*
 Parts List for T-117-CE-LS-W-B

Identification	Description
T-117-CE-LS-W-B-A	Remnant
T-117-CE-LS-W-B-B-1	Remnant
T-117-CE-LS-W-B-B-2	Charpy V-Notch impact specimens (16 total)
T-117-CE-LS-W-B-B-3	Remnant
T-117-CE-LS-W-B-B-4	Remnant
T-117-CE-LS-W-B-B-5	Tensile test specimen
T-117-CE-LS-W-B-B-6	Remnant
T-117-CE-LS-W-B-B-7	Remnant
T-117-CE-LS-W-B-B-8	Chemical analysis specimen
T-117-CE-LS-W-B-B-9	Remnant

*Figure 3a identifies the location of each piece.

Appendix A – Parts List and Preservation

Table 4a*
 Parts List for T-117-CW-LS

Identification	Description
T-117-CW-LS-A	Remnant
T-117-CW-LS-B-1	Remnant
T-117-CW-LS-B-2	Charpy V-notch impact specimens (16 total)
T-117-CW-LS-B-3	Remnant
T-117-CW-LS-B-4	Remnant
T-117-CW-LS-B-5	Tensile test specimen
T-117-CW-LS-B-6	Remnant
T-117-CW-LS-B-7	Remnant
T-117-CW-LS-B-8	Remnant

*Figure 4a identifies the location of each piece.

Appendix A – Parts List and Preservation

Table 5a*
 Parts List for T-117-CW-B

Identification	Description
T-117-CW-B-A	Remnant
T-117-CW-B-B-1	Remnant
T-117-CW-B-B-2	Charpy V-notch impact specimens (16 total)
T-117-CW-B-B-3	Remnant
T-117-CW-B-B-4	Remnant
T-117-CW-B-B-5	Tensile test specimen
T-117-CW-B-B-6	Remnant
T-117-CW-B-B-7	Remnant
T-117-CW-B-B-8	Chemical analysis specimen
T-117-CW-B-B-9	Remnant

*Figure 5a identifies the location of each piece.

Appendix A - Parts List and Preservation

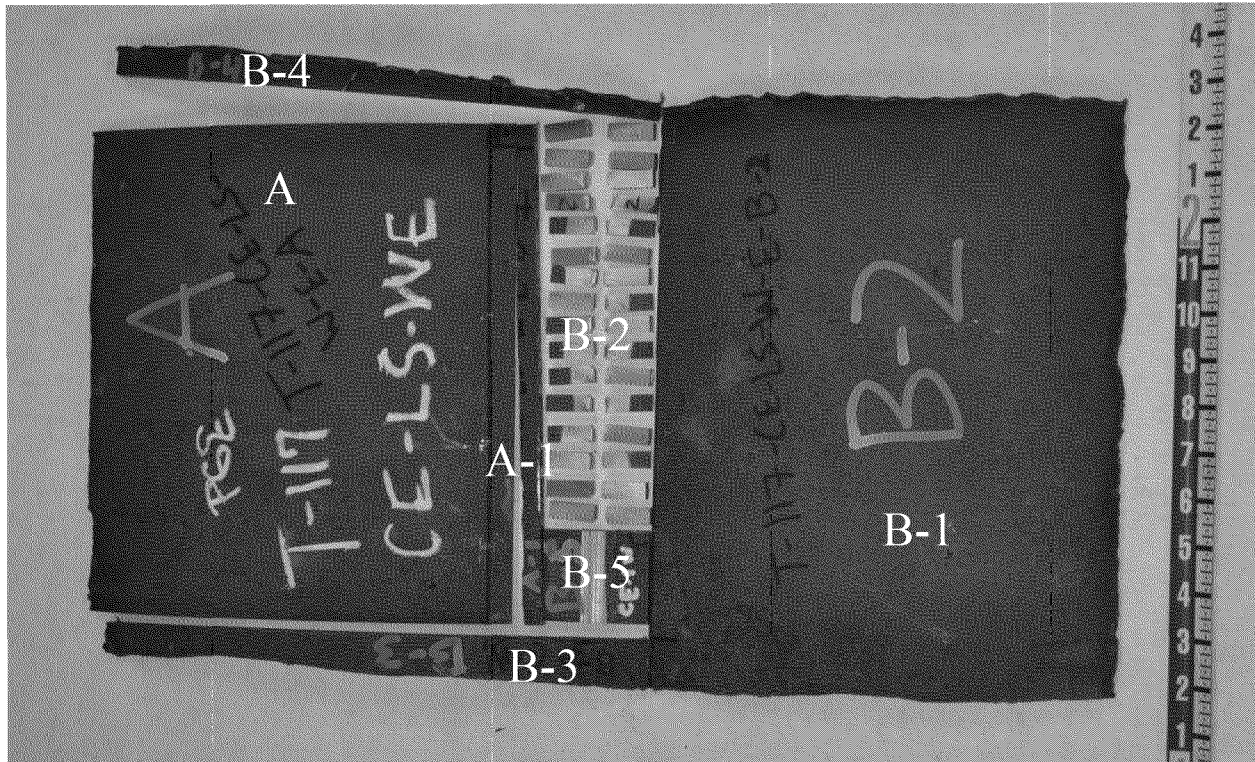


Figure 1a Photograph of the remnants from T-117-CE-LS-W-E.



Appendix A - Parts List and Preservation

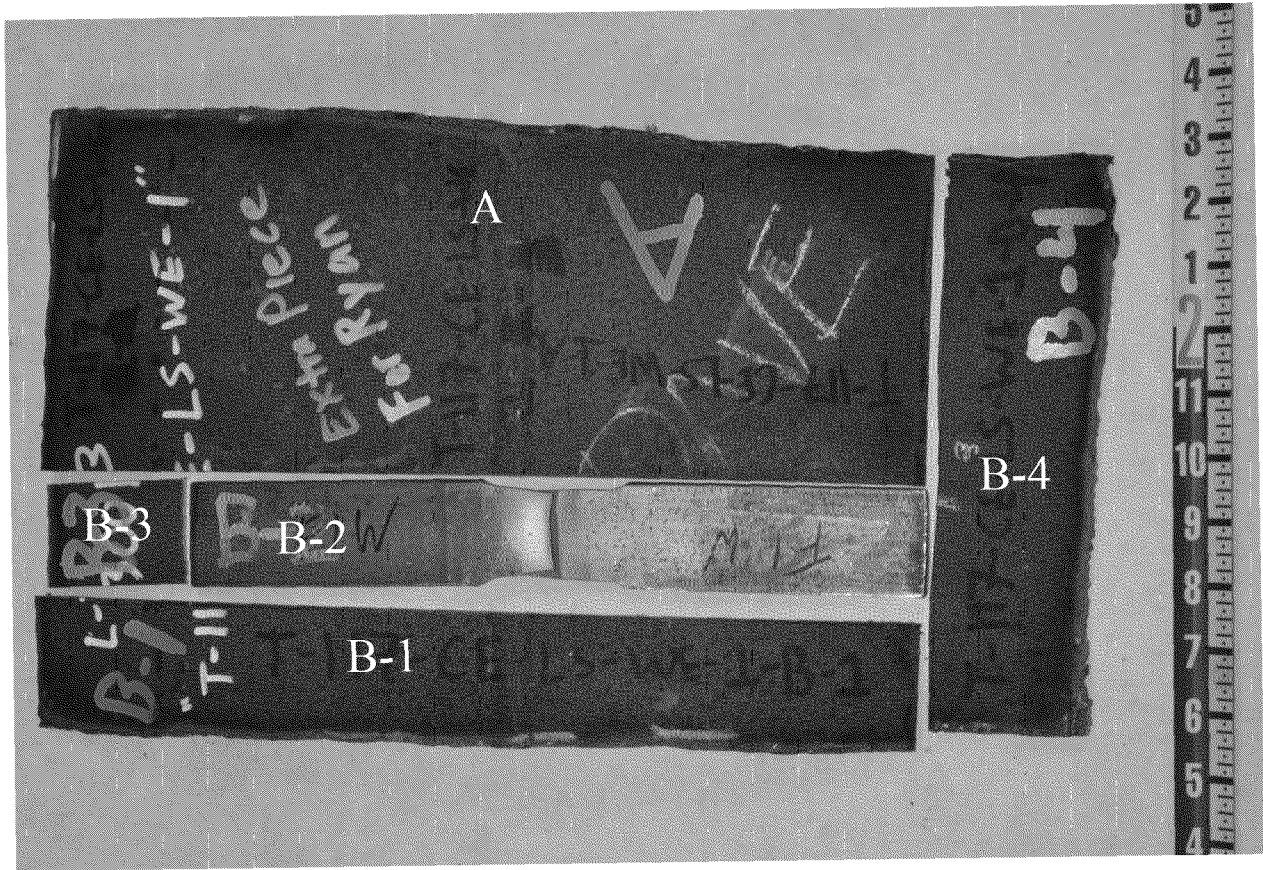


Figure 2a Photograph of remnants from T-117-CE-LS-W-E-1.

Appendix A - Parts List and Preservation

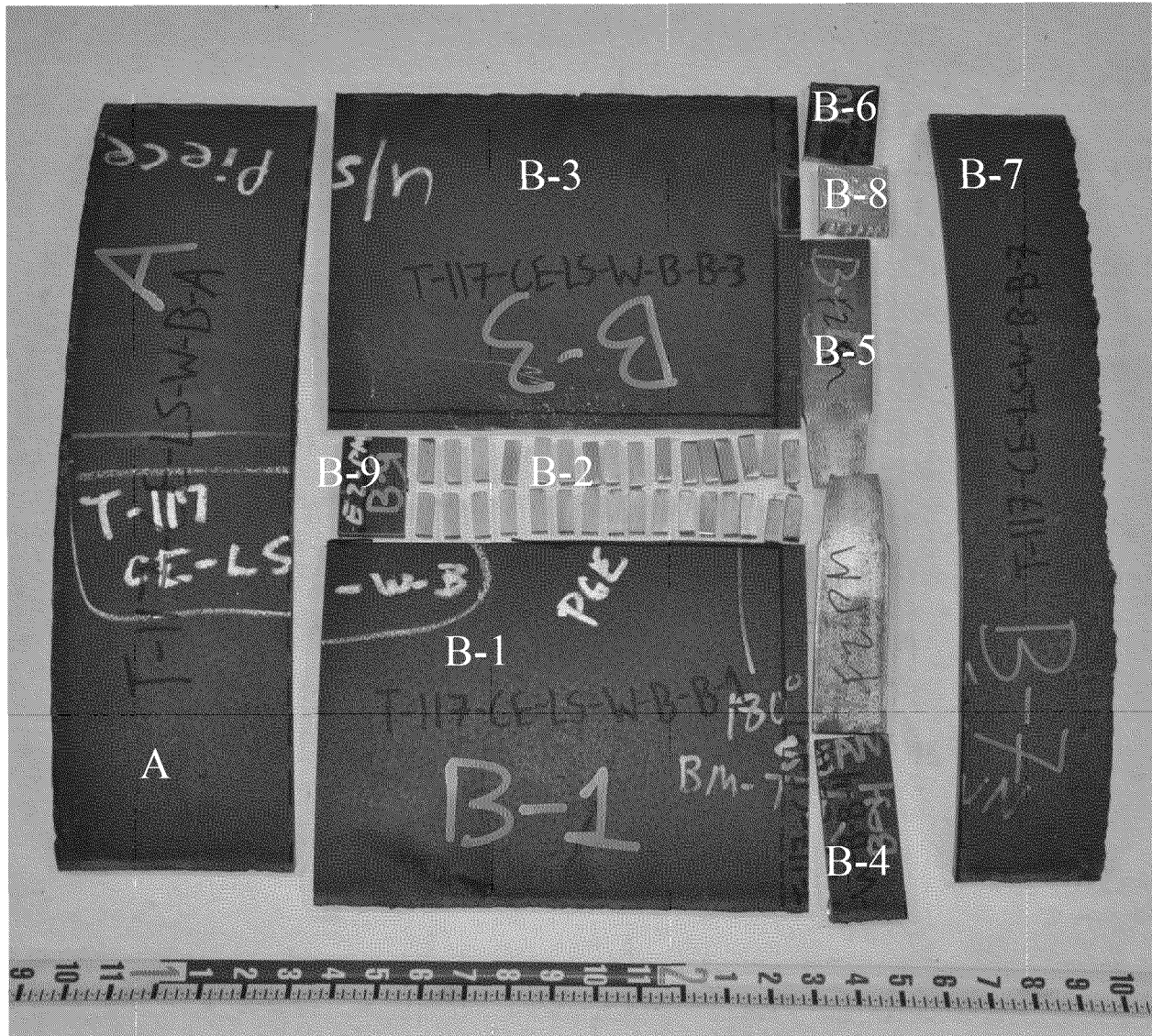


Figure 3a Photograph of remnants from T-117-CE-LS-W-B.

Appendix A - Parts List and Preservation

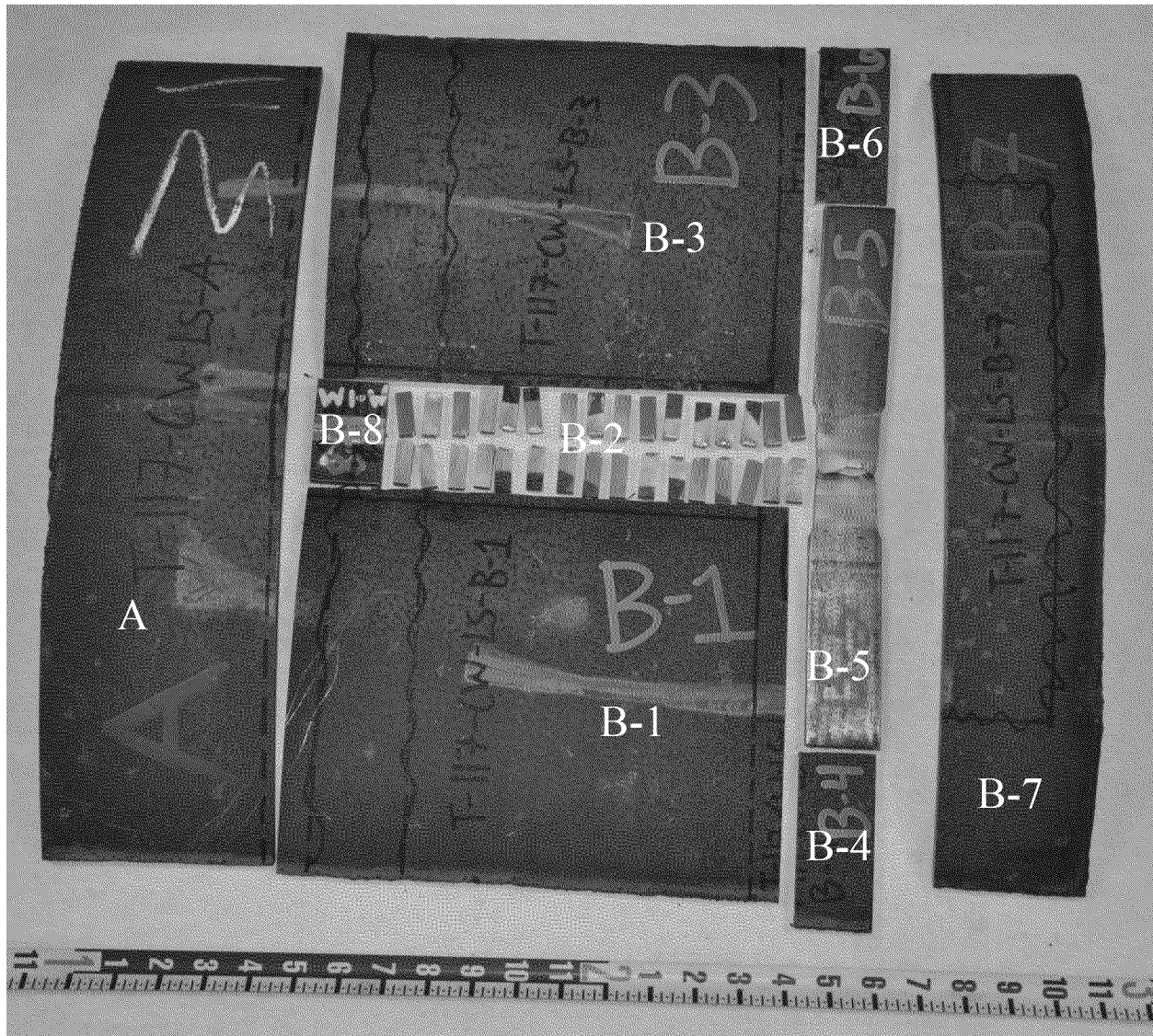


Figure 4a Photograph of the remnants from T-117-CW-LS

Appendix A - Parts List and Preservation

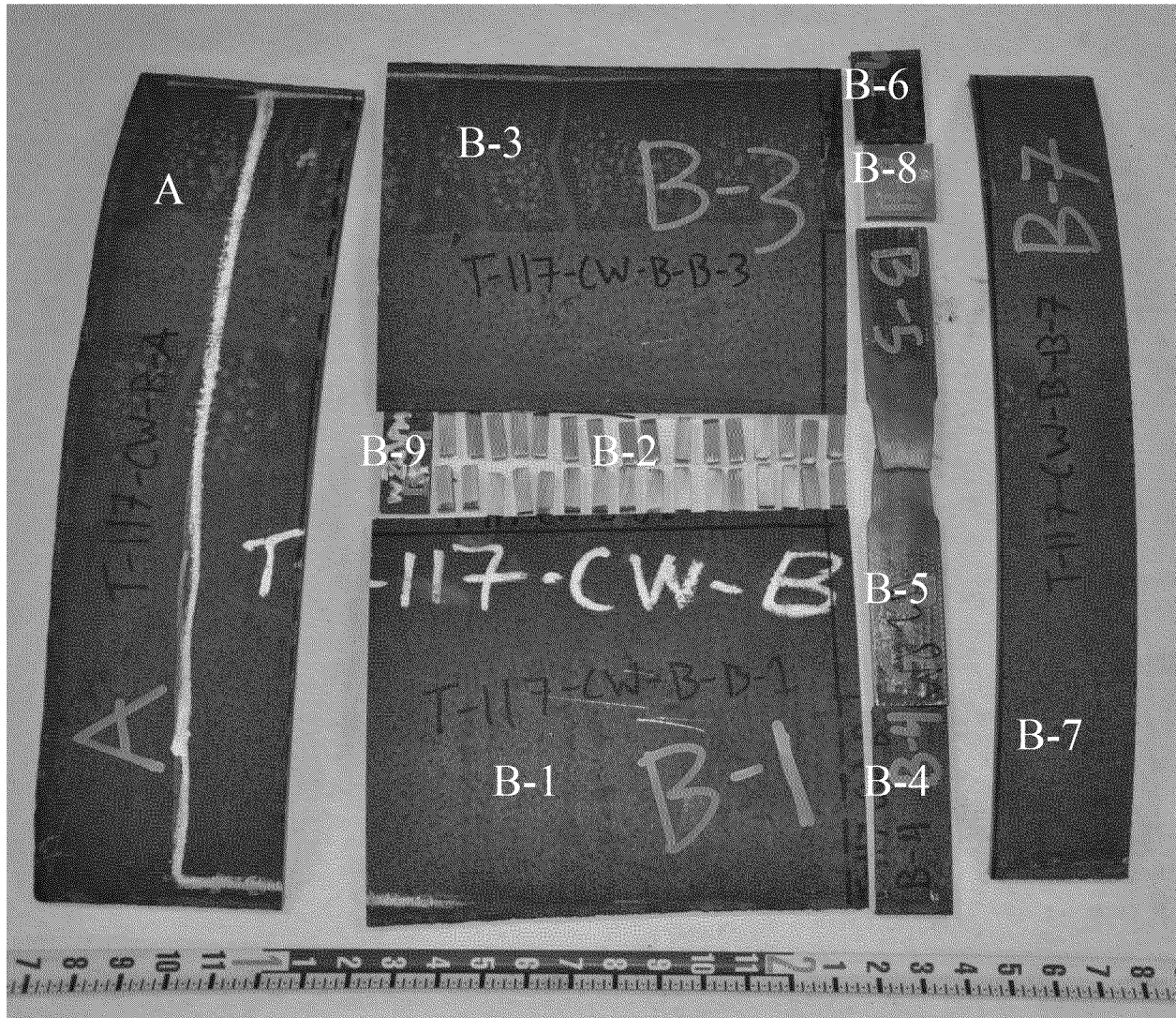


Figure 5a Photograph of the remnants from T-117-CW-B.



Report No. 5004.7022

March 7, 2012

**MECHANICAL TESTING AND CHEMICAL ANALYSIS OF FOUR PIPE
SECTIONS FROM LINE 300B MP 285 HYDRO TEST FAILURE
– ADDITIONAL TESTING**

Customer Authorization: CWA # 2500614261

Report To: Pacific Gas and Electric Company
ATTN: Dave Aguiar
375 North Wiget Lane, Suite 250
Walnut Creek, CA 94958

REPORT

Four pipe sections from Pacific Gas and Electric, Walnut Creek, CA were submitted for mechanical testing and chemical analysis. The samples were from “Line 300B MP 285 Hydro Test Failure – Additional Testing”. The samples were identified by PG&E as: T-117-1-E-LS, T-117-1-E-BM, T-117-2-W-LS, and T-117-2-W-BM. Photographs of the samples as-received are shown in Figure 1 through Figure 4.

Tensile testing was conducted on the longitudinal seam weld of T-117-1-E-LS and T-117-2-W-LS and the base metal of T-117-1-E-BM and T-117-2-W-BM. All of the tensile testing was conducted per API 5L¹. The tensile test specimens were oriented in the circumferential direction. The results of the tensile tests are listed in Table 1.

Charpy V-notch impact testing was conducted on the longitudinal seam weld of T-117-1-E-LS and T-117-2-W-LS and the base metal of T-117-1-E-BM and T-117-2-W-BM. The charpy V-notch impact specimens were oriented in the circumferential direction with the notch in the axial direction. The dimensions of all of the charpy V-notch impact specimens was 8.0 mm x 10 mm x 55 mm (thickness x width x length). The results of the charpy V-notch impact tests are listed in Table 2 through Table 5.

Quantitative chemical analysis was completed on the base metal from samples T-117-1-E-BM and T-117-2-W-BM. The results of the chemical analysis are listed in Table 6.

The samples T-117-1-E-LS and T-117-2-W-LS were sectioned through the longitudinal seam welds and the specimens were prepared for metallography. The locations where the samples were obtained are shown in Figure 1 and Figure 3. Photographs of the metallographic sections are shown in Figure 5.

¹ API 5L – *Specification of Line Pipe*, 2007.

This report shall not be reproduced, except in full, without the written approval of Anamet.

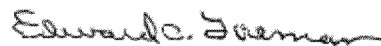
This testing was completed on March 7, 2012 and was performed in accordance with the customer's authorization.

Prepared by:



Ryan Wood
Materials Engineer

Reviewed by:



Edward Foreman
Quality Manager

Table 1
 Results of the Tensile Tests
 (ASTM A 370-10)

	Tensile Strength (ksi)	Yield Strength 0.5% EUL (ksi)	Elongation in 2-inches (%)	Fracture Location
T-117-1-E-LS	88.8	69.3	20.5	Base Metal
T-117-1-E-BM	85.6	67.8	30.5	n/a
T-117-2-W-LS	89.0	71.6	18.5	Base Metal
T-117-2-W-BM	88.3	66.0	29.5	n/a

Table 2
 Results of the Charpy V-Notch Impact Tests
 of T-117-1-E-LS
 (ASTM A 370-10)

Temperature	Energy Absorbed (ft lb)	Lateral Expansion (mils)	Shear (%)
+32 °F	9	14	23
	7 ½	15	37
	8	13	32
+50 °F	9 ½	20	46
	8 ½	16	37
	9 1/2	18	32

Table 3
 Results of the Charpy V-Notch Impact Tests
 of T-117-1-E-BM
 (ASTM A 370-10)

Temperature	Energy Absorbed (ft lb)	Lateral Expansion (mils)	Shear (%)
+32 °F	11 ½	18	23
	9 ½	16	18
	11	17	25
+50 °F	14 ½	24	40
	13	19	34
	15	25	38

Table 4
 Results of the Charpy V40-Notch Impact Tests
 of T-117-2-W-LS
 (ASTM A 370-10)

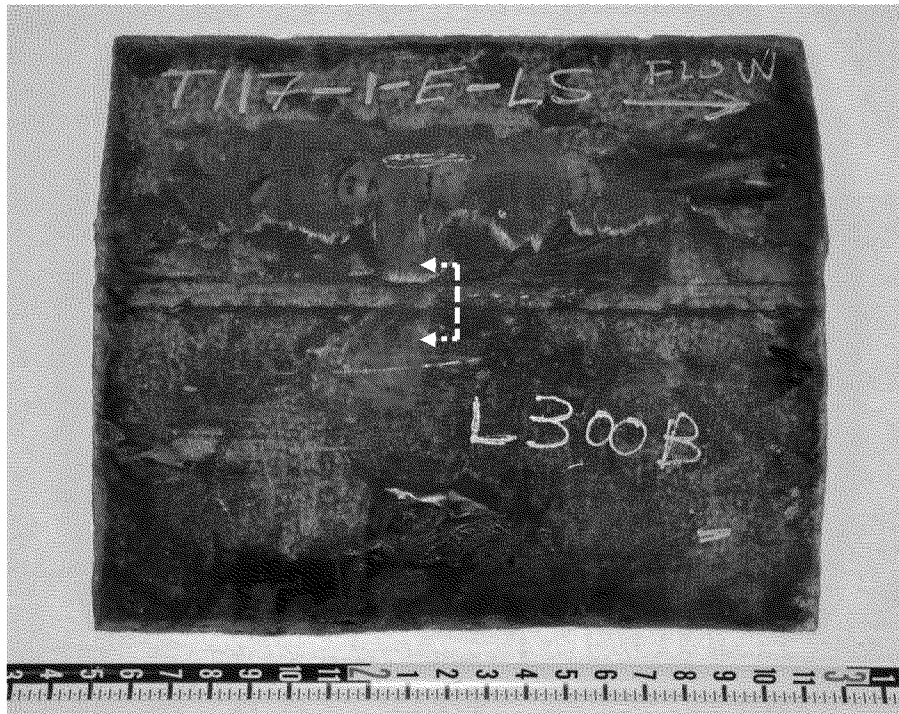
Temperature	Energy Absorbed (ft lb)	Lateral Expansion (mils)	Shear (%)
+32 °F	7	11	42
	7	11	47
	9	16	18
+50 °F	9	13	25
	12	17	42
	12	18	28

Table 5
 Results of the Charpy V-Notch Impact Tests
 of T-117-2-W-BM
 (ASTM A 370-10)

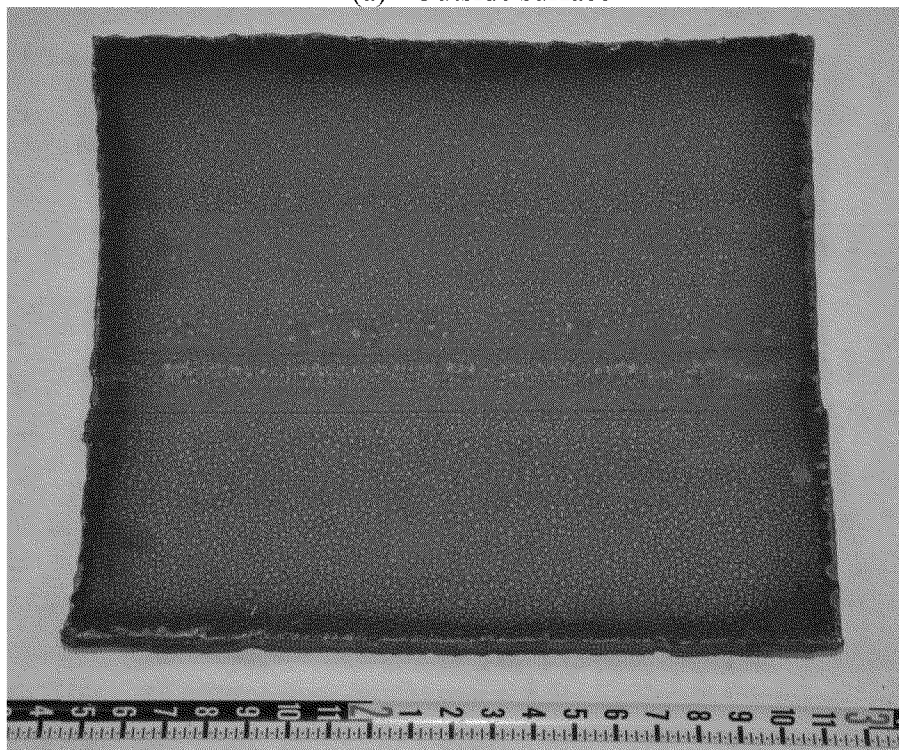
Temperature	Energy Absorbed (ft lb)	Lateral Expansion (mils)	Shear (%)
+32 °F	13 ½	17	18
	9	14	18
	10 ½	15	23
+50 °F	14	20	32
	13 ½	19	32
	17	23	28

Table 6
 Results of Quantitative Chemical Analysis of
 T-117-1-E-BM and T-117-2-W-BM

Element	T-117-1-E-BM (weight %)	T-117-2-W-BM (weight %)
Carbon (C)	0.29	0.30
Chromium (Cr)	0.01	0.03
Columbium (Cb)	<0.005	<0.005
Copper (Cu)	0.08	0.09
Iron (Fe)	Main Constituent	Main Constituent
Manganese (Mn)	1.02	1.03
Molybdenum (Mo)	<0.005	<0.005
Nickel (Ni)	0.08	0.08
Phosphorus (P)	0.012	0.023
Silicon (Si)	0.07	0.06
Sulfur (S)	0.055	0.040
Titanium (Ti)	<0.005	<0.005
Vanadium (V)	<0.005	<0.005

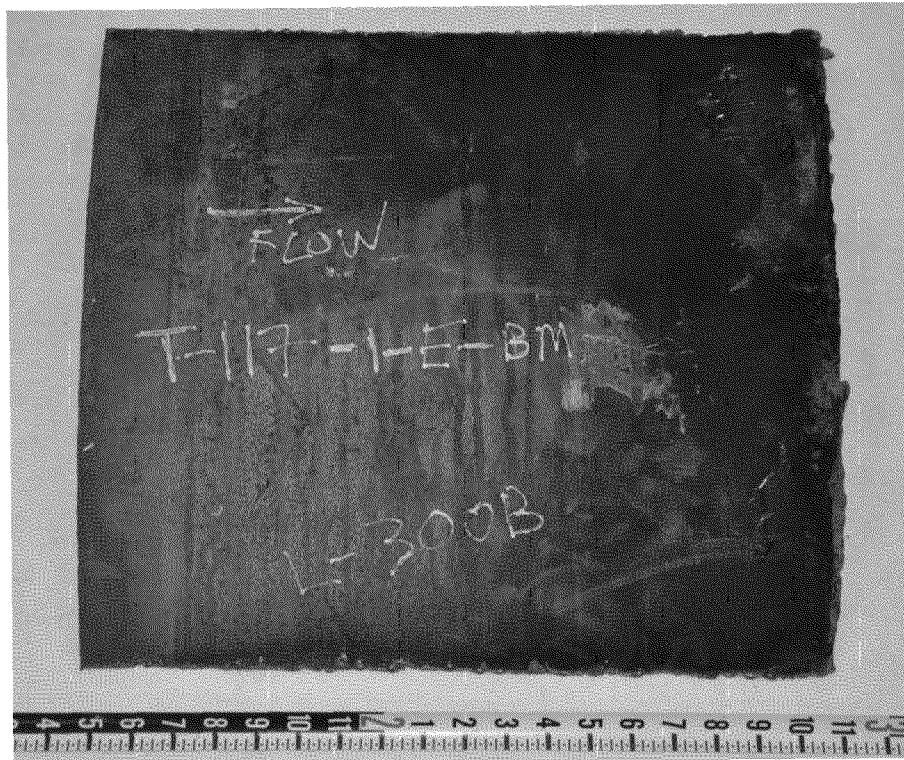


(a) Outside surface

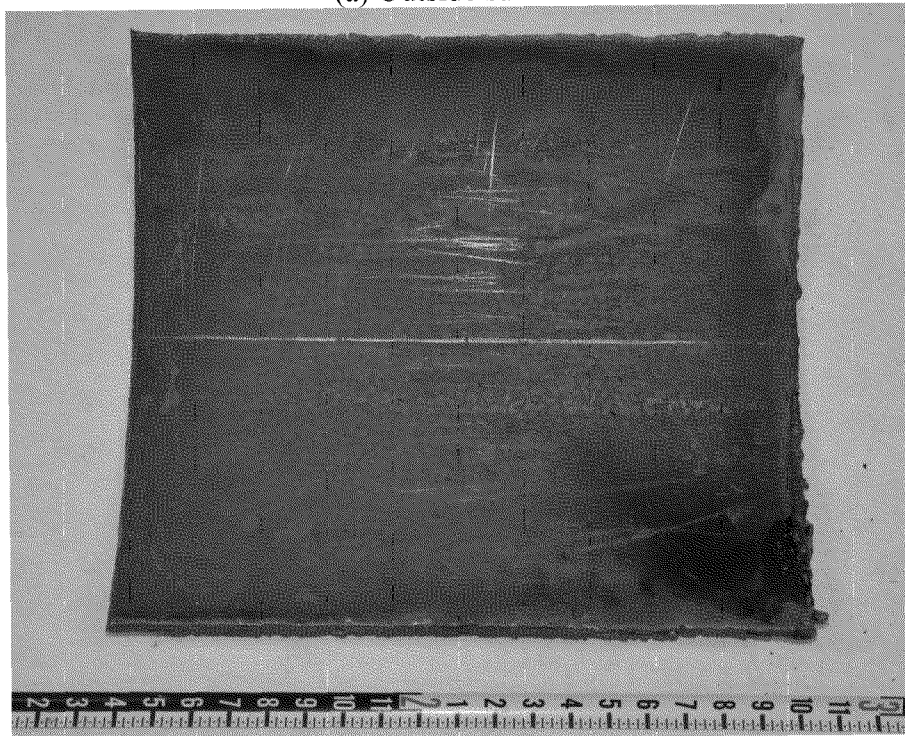


(b) Inside surface

Figure 1 Photographs of T-117-1-E-LS as-received. (a) The white dashed lines indicate where the metallographic specimen was obtained.

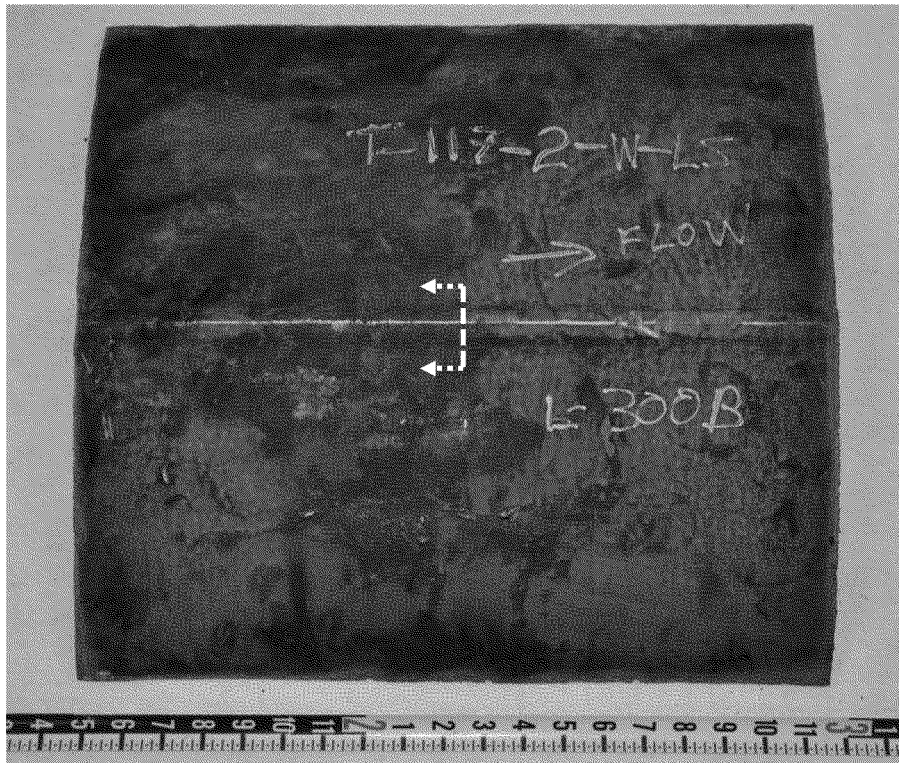


(a) Outside surface

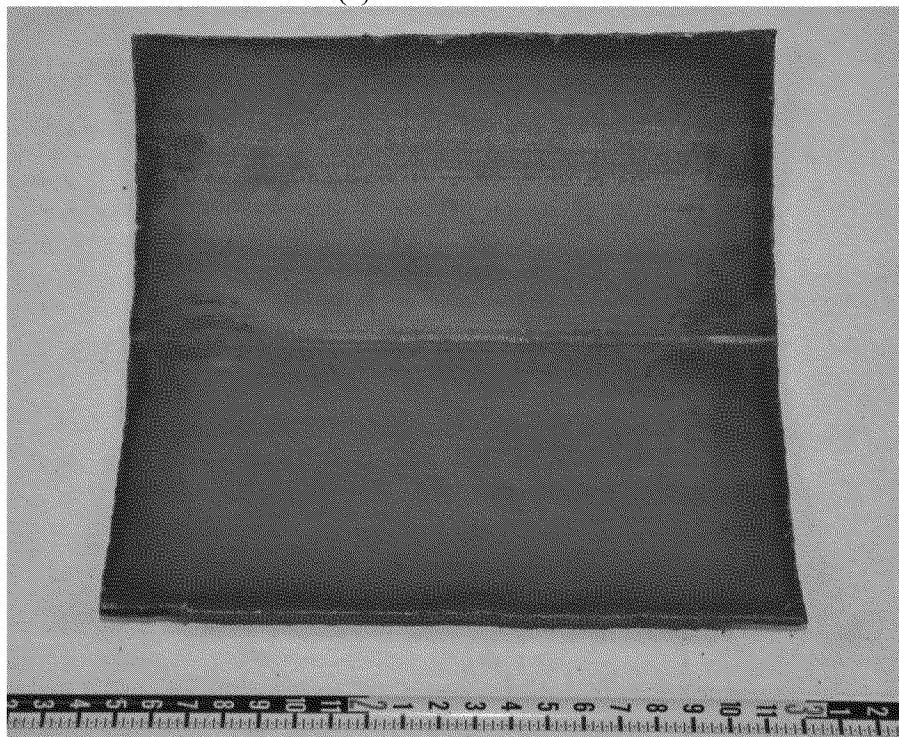


(b) Inside surface

Figure 2 Photographs of T-117-1-E-BM as-received.

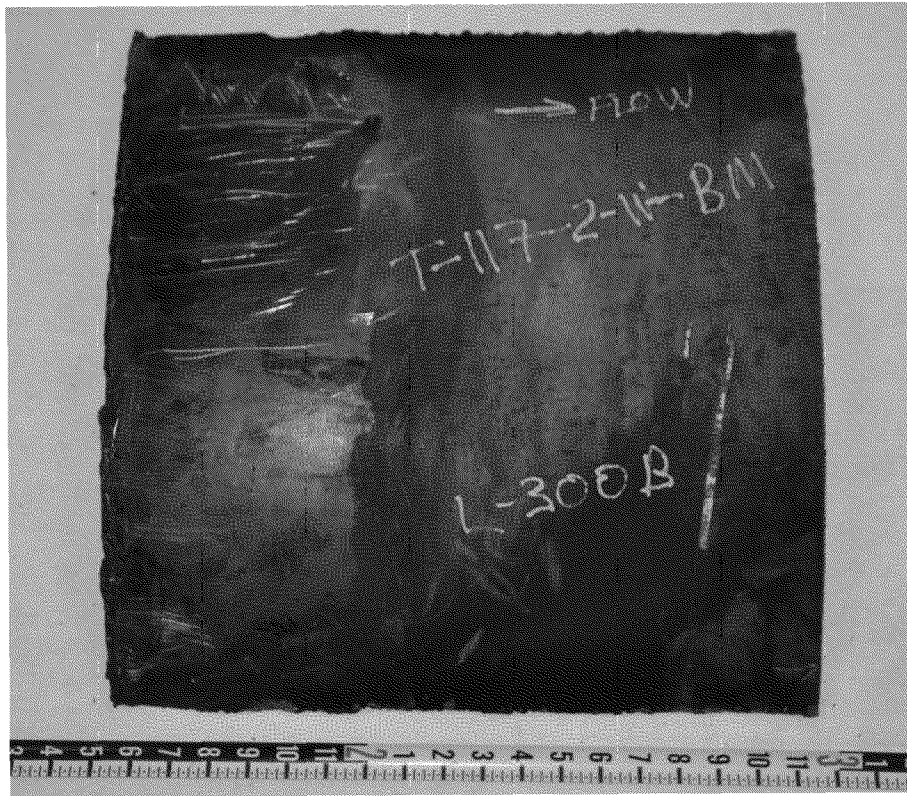


(a) Outside surface



(b) Inside surface

Figure 3 Photographs of T-117-2-W-LS as-received. (a) The white dashed lines indicate where the metallographic specimen was obtained.

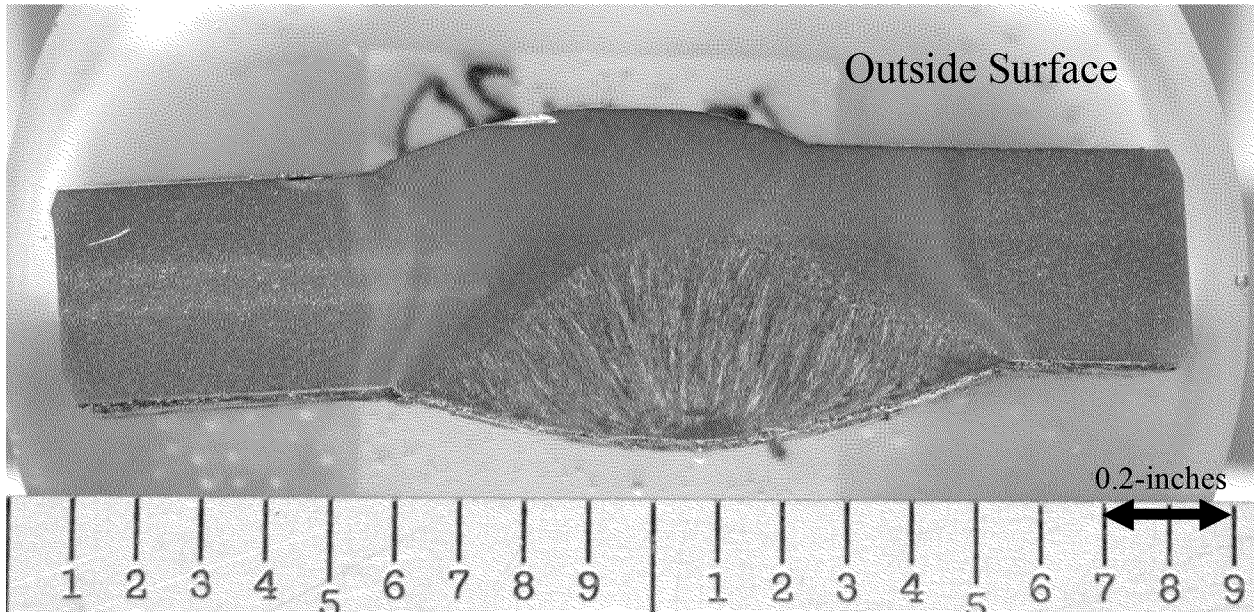


(a) Outside surface

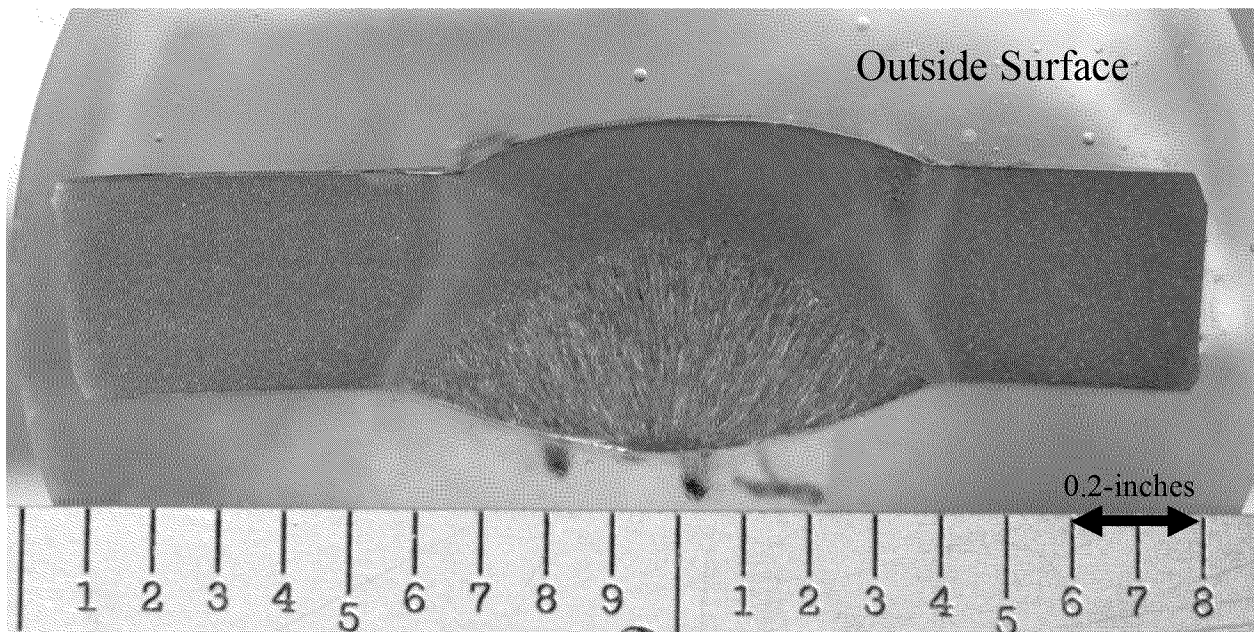


(b) Inside surface

Figure 4 Photographs of T-117-2-W-BM as-received.



(a) T-117-1-E-LS



(b) T-117-2-W-LS

Figure 5 Photographs of the metallographic sections.

Appendix A – Parts List and Preservation

Table 1a*
 Parts List for T-117-1-E-LS

Identification	Description
T-117-1-E-LS-A	Remnant
T-117-1-E-LS-B-1	Remnant
T-117-1-E-LS-B-2	Metallographic section
T-117-1-E-LS-B-2-A	Remnant
T-117-1-E-LS-B-3	Remnant
T-117-1-E-LS-B-4	Remnant
T-117-1-E-LS-B-5	Charpy V-notch impact test specimens (6 total)
T-117-1-E-LS-B-6	Remnant
T-117-1-E-LS-B-7	Remnant
T-117-1-E-LS-B-8	Tensile test specimen
T-117-1-E-LS-B-9	Remnant

*Figure 1a identifies the location of each piece.

Appendix A - Parts List and Preservation

Table 2a*
 Parts List for T-117-1-E-BM

Identification	Description
T-117-1-E-BM-A	Remnant
T-117-1-E-BM-B-1	Remnant
T-117-1-E-BM-B-2	Charpy V-notch impact test specimens (6 total)
T-117-1-E-BM-B-3	Remnant
T-117-1-E-BM-B-4	Remnant
T-117-1-E-BM-B-5	Tensile test specimen
T-117-1-E-BM-B-6	Chemical analysis specimen
T-117-1-E-BM-B-7	Remnant
T-117-1-E-BM-B-8	Remnant

*Figure 2a identifies the location of each piece.

Appendix A – Parts list and Preservation

Table 3a*
 Parts List for T-117-2-W-LS

Identification	Description
T-117-2-W-LS-A	Remnant
T-117-2-W-LS-B-1	Remnant
T-117-2-W-LS-B-2	Charpy V-notch impact test specimens (6 total)
T-117-2-W-LS-B-3	Remnant
T-117-2-W-LS-B-4	Metallographic specimen
T-117-2-W-LS-B-4-A	Remnant
T-117-2-W-LS-B-5	Remnant
T-117-2-W-LS-B-6	Tensile test specimen
T-117-2-W-LS-B-7	Remnant
T-117-2-W-LS-B-8	Remnant
T-117-2-W-LS-B-9	Remnant
T-117-2-W-LS-B-10	Remnant

*Figure 3a identifies the location of each piece.

Appendix A – Parts List and Preservation

Table 4a*
 Parts List for T-117-2-W-BM

Identification	Description
T-117-2-W-BM-A	Remnant
T-117-2-W-BM-B-1	Remnant
T-117-2-W-BM-B-2	Charpy V-notch impact test specimens (6 total)
T-117-2-W-BM-B-3	Remnant
T-117-2-W-BM-B-4	Remnant
T-117-2-W-BM-B-5	Tensile test specimen
T-117-2-W-BM-B-6	Chemical analysis specimen
T-117-2-W-BM-B-7	Remnant
T-117-2-W-BM-B-8	Remnant

*Figure 4a identifies the location of each piece.

Appendix A - Parts List and Preservation

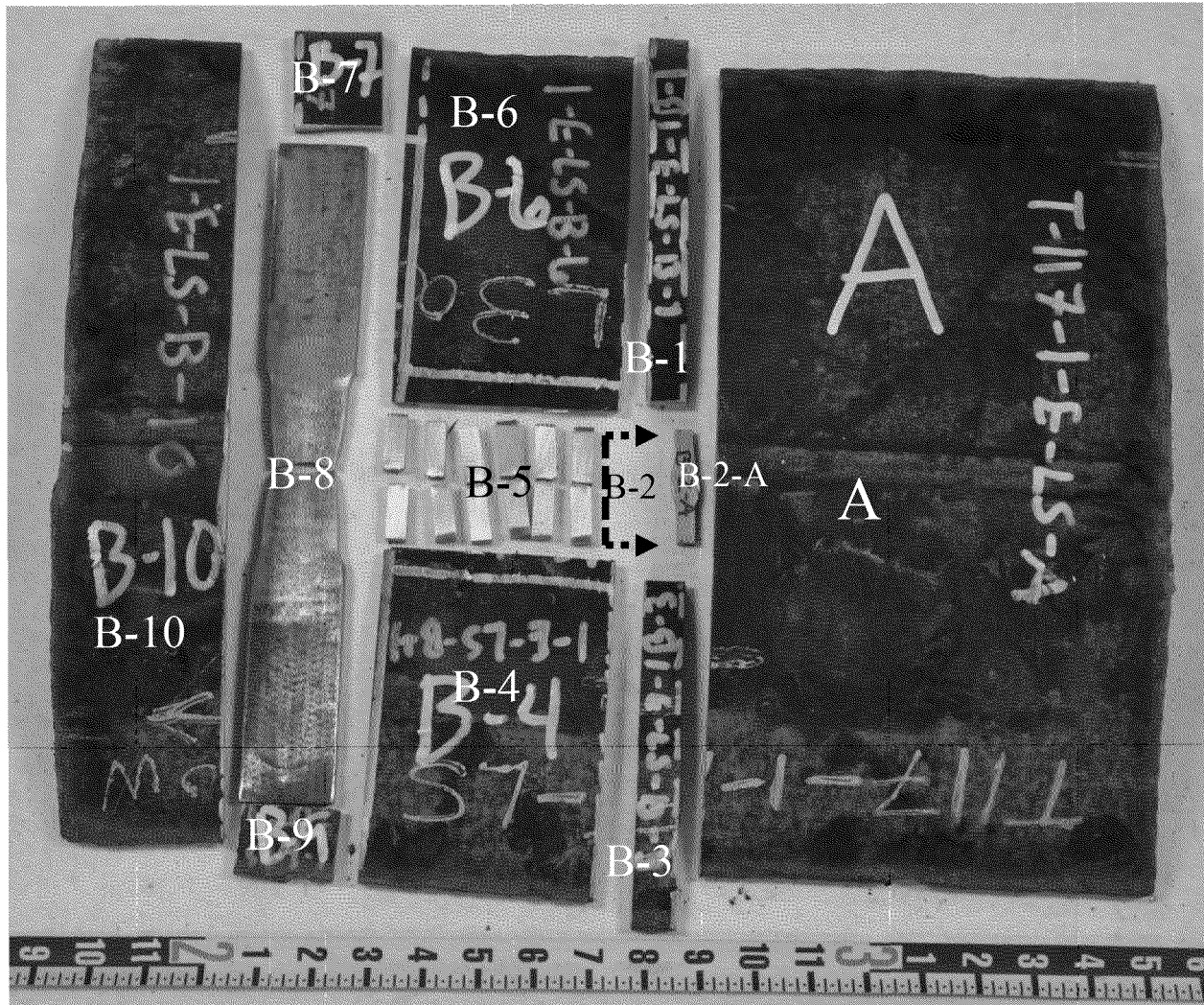


Figure 1a Photograph of the remnants from T-117-1-E-LS. The black dashed lines identified as "B-2" indicate where the metallographic specimen was obtained.

Appendix A - Parts List and Preservation

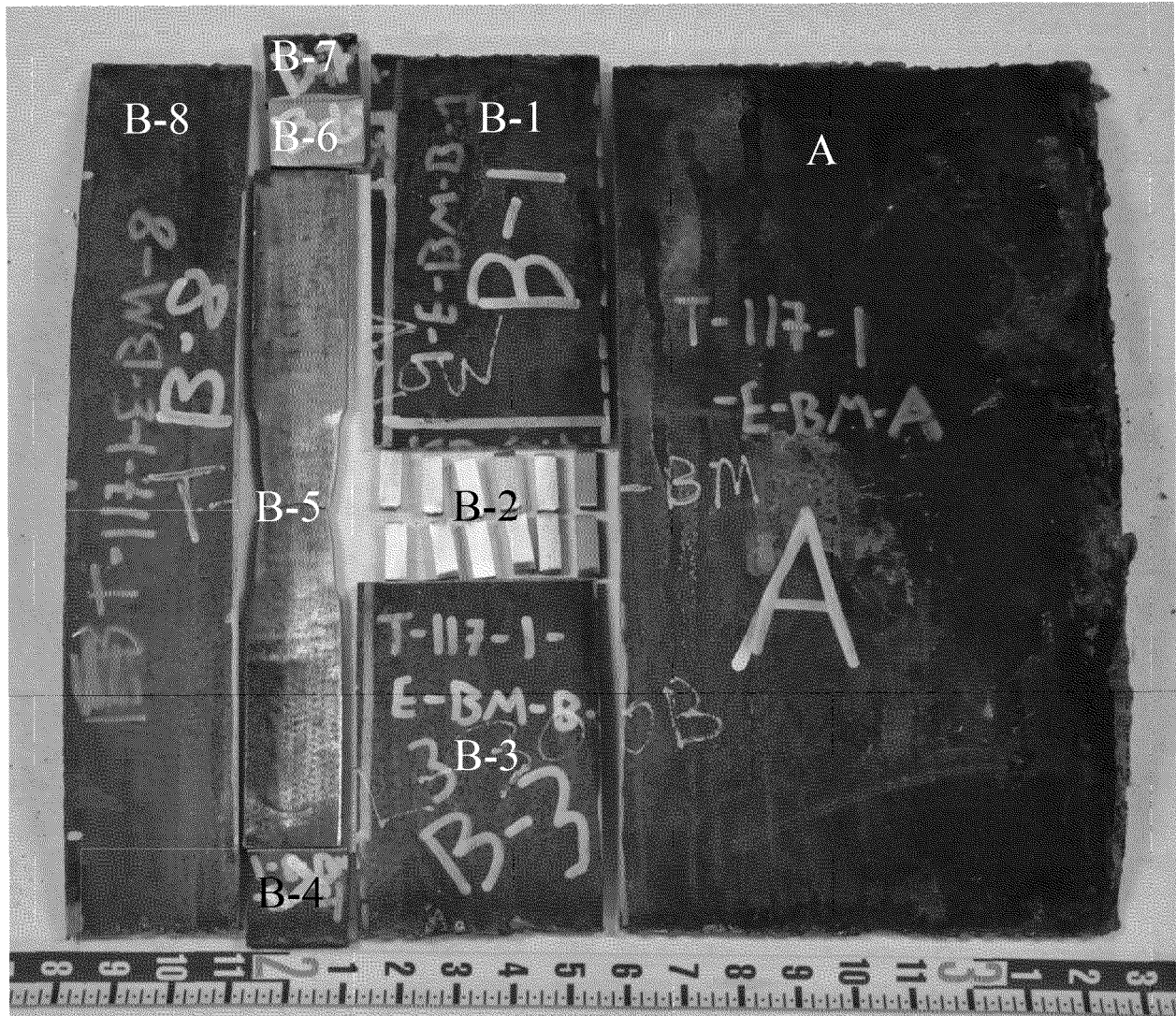


Figure 2a Photograph of remnants from T-117-1-E-BM.

Appendix A - Parts List and Preservation

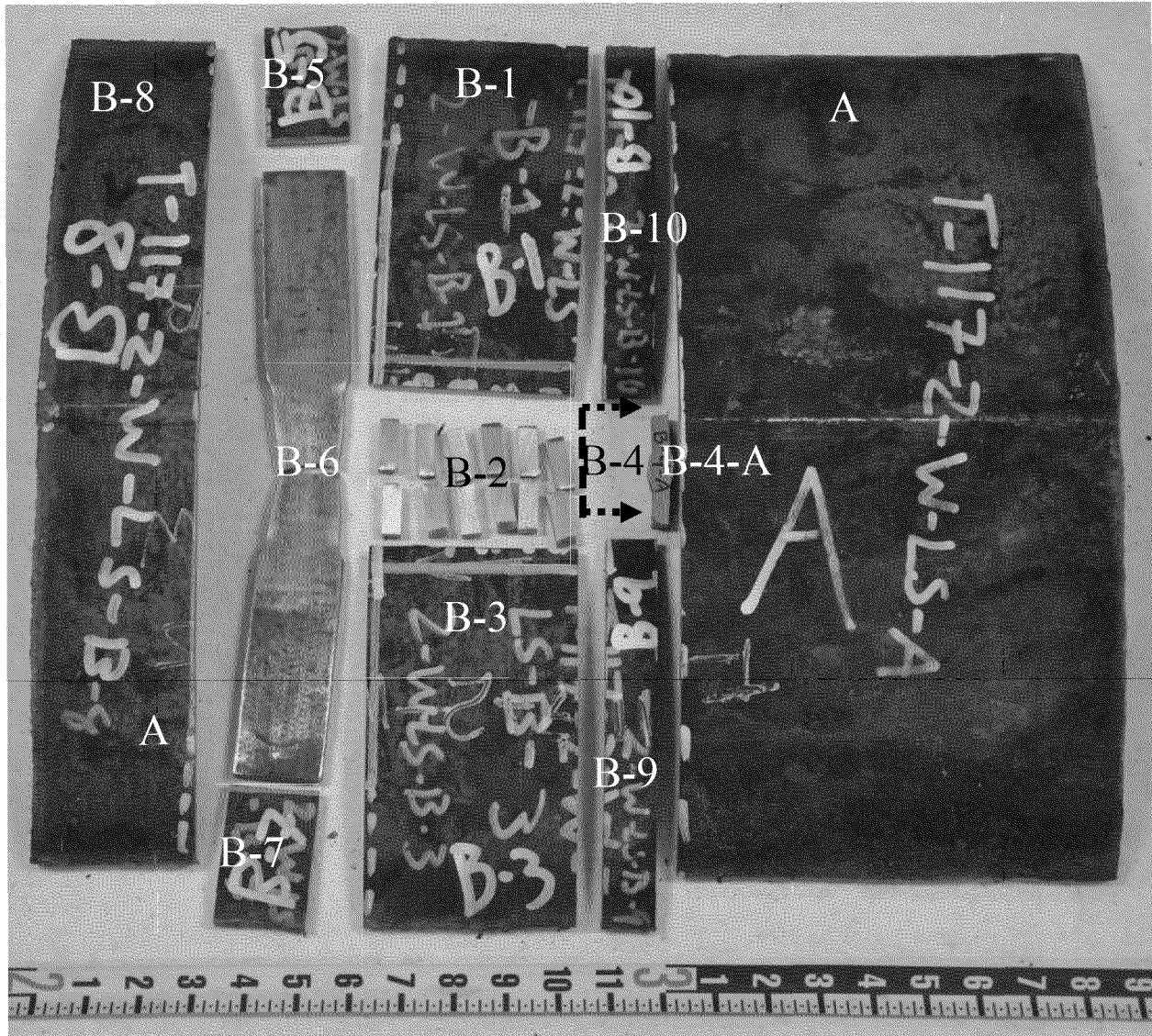


Figure 3a Photograph of remnants from T-117-2-W-LS. The black dashed lines identified as "B-4" indicate where the metallographic specimen was obtained.

Appendix A - Parts List and Preservation

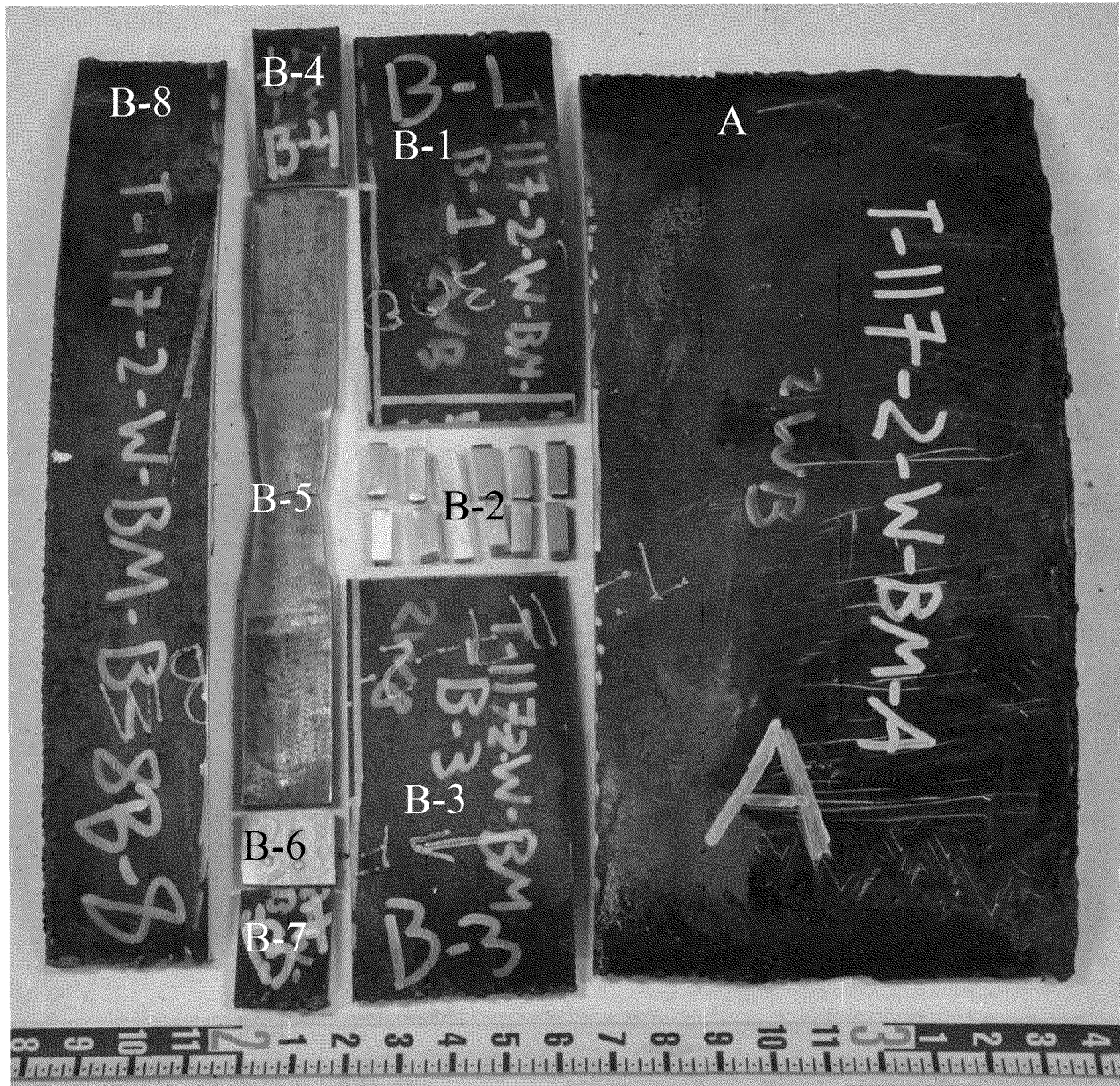


Figure 4a Photograph of the remnants from T-117-2-W-BM